

Scalable Deep Metric Learning on Attributed Graphs

Xiang Li¹, Gagan Agrawal², Ruoming Jin³, and Rajiv Ramnath¹

¹ The Ohio State University, Columbus OH 43210, USA

² University of Georgia, Athens GA 30602, USA

³ Kent State University, Kent OH 44242, USA

Abstract. We consider the problem of constructing embeddings of large attributed graphs and supporting multiple downstream learning tasks. We develop a graph embedding method, which is based on extending deep metric and unbiased contrastive learning techniques to 1) work with attributed graphs, 2) enabling a mini-batch based approach, and 3) achieving scalability. Based on a multi-class triplet loss function, we present two algorithms – DMT for semi-supervised learning and DMAT-i for the unsupervised case. Analyzing our methods, we provide a generalization bound for the downstream node classification task and for the first time relate triplet loss to contrastive learning. Through extensive experiments, we show high scalability of representation construction, and in applying the method for three downstream tasks (node clustering, node classification, and link prediction) better consistency over any single existing method.

Keywords: Attributed Graph · Deep Metric Learning · Graph Embedding · Graph Convolutional Network · Scalability

1 Introduction

Last several years have seen much interest in developing learning techniques on *attributed graphs*, i.e., graphs with features associated with nodes. Such graphs are seen in multiple domains such as recommendation systems [52], analysis of citation or social networks [39,19], and others. Of particular interest are the deep learning based graph embedding methods [38,54,57,9,58] that encode graph structural information and node features into low-dimensional representations for multiple downstream tasks. Current approaches use Graph Convolutional Networks (GCN) [58] or graph filters [54,57,9], but either way, the methods do not scale to large graphs. At a high level, these graph embeddings are designed with the primary objective of pulling examples with distinct labels apart from each other, while pushing the ones sharing the same label closer. It turns out that the spirit of deep metric learning [33,28] is also almost the same, though to date this idea has been primarily applied to learn visual representations [4,56,25]. However, besides the challenges of tailoring these methods for attributed graphs, scalability is also a concern. Specifically, deep metric learning requires: 1) explicit sampling of triplets such that one or more negative examples is against a single

positive example [28], and 2) expensive search to increase negative hardness of samples, which is needed for enhanced learning power [33,10,27].

This paper addresses these problems in applying deep metric learning to attributed graphs in a scalable fashion. First, we employed an extended version of *multi-class triplet loss* function [36] capable of working with multiple positive samples, building on a similar loss function has been discussed in [17] for image classification. Next, we use (approximate) Generalized PageRank (GPR) [5] as a scalable graph filter, which also leads to a compact node representation and, as we observe, increased negative sample hardness. Finally, we further achieve scalability by mini-batch training; specifically with each batch serving as a natural tuple comprising multiple positive and negative samples; and eliminate the cost of sampling. With this basic framework, we build multiple algorithms, specifically, **Deep Metric Learning with Multi-class Triplet Loss (DMT)** for semi-supervised learning and **DMAT-i** for unsupervised conditions.

To summarize the novelty of our contributions – we connect DMAT-i with an extensively applied contrastive loss [6] and theoretically establish how it leads to a bound on the generalization error of a downstream classification task. Equally important, our theoretical analysis explains why contrastive learning is successful for graph representation learning from a deep metric learning perspective. On the experimental side, we compare our methods with the state-of-the-art baselines in semi-supervised node classification, node clustering, and link prediction, and show more consistent level of accuracy as compared to any existing method, and state-of-the-art results in several cases. Finally, we also show greater scalability with our methods.

2 Preliminaries

Deep Metric Learning. We denote $x \in \mathcal{X}$ as the input data, with corresponding labels $y \in \mathcal{Y}$. Let $\mathcal{C}: \mathcal{X} \rightarrow \mathcal{Y}$ be the function of assigning these labels, i.e., $y = \mathcal{C}(x)$. In deep metric learning, we denote x^+ as a *positive sample* of x (i.e., $\mathcal{C}(x^+) = \mathcal{C}(x)$) and x^- as the *negative sample* (i.e., $\mathcal{C}(x^-) \neq \mathcal{C}(x)$). Define $p_x^+(x')$ to be the probability of observing x' as a positive sample of x and $p_x^-(x')$ the probability its being a negative sample. We assume the class probabilities are uniform such that probability of observing y as a label is τ^+ and probability of observing any different class is $\tau^- = 1 - \tau^+$. Then the data distribution can be decomposed as $p(x') = \tau^+ p_x^+(x') + \tau^- p_x^-(x')$.

Deep metric learning uses a neural network $f: \mathcal{X} \rightarrow \mathbb{R}^d$ to learn a d -dimensional nonlinear embedding $f(x)$ for each example x based on objectives such as triplet loss [36] or triplet loss [33]. [36] proposed a $(N+1)$ -tuple loss, where for a tuple $(x, x^+, \{x_i^-\}_{i=1}^{N-1})$ we optimize to identify a single positive example from multiple negative examples as:

$$L_{\text{tuple}}^{N+1}(f) = \log \left(1 + \sum_{i=1}^{N-1} \exp \{ f(x)^\top f(x_i^-) - f(x)^\top f(x^+) \} \right) \quad (1)$$

This softmax function based objective is *hardness known* where the hard negative samples receive larger gradients [11].

Contrastive Learning. In fact, $L_{\text{tuple}}^{\mathcal{N}+1}$ is mathematically equal to the ideal *unbiased contrastive loss* $\tilde{L}_{\text{Unbiased}}^{\mathcal{N}+1}(f)$ proposed in [8], where they introduced:

$$\tilde{L}_{\text{Unbiased}}^{\mathcal{N}+1}(f) = -\log \frac{\exp\{f(x)^\top f(x^+)\}}{\exp\{f(x)^\top f(x^+)\} + (\mathcal{N}-1) \mathbb{E}_{x^- \sim p_x^-} \exp\{f(x)^\top f(x^-)\}} \quad (2)$$

In contrastive learning, the positive sample (and negative samples) are obtained through perturbation and mainly used in the unsupervised setting (where class label is not available). Thus, p_x^- is usually not accessible and negative samples x_i^- are generated from the (unlabeled) $p(x)$ [8]. Thus, the typical contrastive loss [6] now becomes:

$$\tilde{L}_{\text{Contrast}}^{\mathcal{N}+1}(f) = -\log \frac{\exp\{f(x)^\top f(x^+)\}}{\exp\{f(x)^\top f(x^+)\} + (\mathcal{N}-1) \mathbb{E}_{x^- \sim p} \exp\{f(x)^\top f(x^-)\}} \quad (3)$$

Since x_i^- is drawn from $p(x)$, it also has a probability of τ^+ of being a positive sample. Thus, the contrastive learning is closely related to, and can even be considered a variant of, deep metric learning, where the positive/negative samples are generated through different perturbation mechanisms. To facilitate our discussion, we use the notations $L_{\text{tuple}}^{\mathcal{N}+1}$ and $\tilde{L}_{\text{Unbiased}}^{\mathcal{N}+1}$ interchangeably in the rest of the paper. More related works are reviewed in appendix.

3 Methodology

3.1 Problem Statement

We are given an attributed graph $\mathcal{G} = (\mathcal{V}, \mathcal{E}, \tilde{X})$, where $\mathcal{V} = \{v_1, v_2, \dots, v_N\}$ and \mathcal{E} represent node set and edge set, respectively, and \tilde{X} denotes the node attributes (i.e., each node is associated with a feature vector). Each vertex v_i belongs to a single class (or a cluster) and we apply all notations defined in deep metric learning to graph representations. The input data for deep metric learning \mathcal{X} is calculated by a graph filter \mathcal{H} : $\mathcal{X} = \mathcal{H}(\tilde{X}, A)$, where A is the adjacency matrix. Our objective is to learn an encoder $f: \mathcal{X} \rightarrow \mathbb{R}^d$ to obtain a d -dimensional embedding $f(\mathcal{X})$.

To develop deep metric learning (or contrastive learning) on graphs, we need to consider and address the following problems: (1) How to establish a unified approach to cover both semi-supervised and unsupervised settings for graphs? (2) How to scale the learning process for large-scale graphs by taking advantage of mini-batch training?

To elaborate on the second point, the existing contrastive learning for graph representation, particularly GCA [58], is built upon a GCN architecture and uses a typical contrastive loss [6]. It perturbs the graph topology and node attributes separately, which are fed to GCN to generate augmented views for contrasting. The transformation by GCN limits both accuracy (due to over-smoothing [21]) and scalability.

3.2 DMT Algorithm

We first propose the learning framework, **Deep Metric Learning with Multi-class Tuple** (**DMT**), for semi-supervised node classification task. By applying a multiclass tuple loss [36,17] which can recognize multiple positive samples from

the tuple, DMT addresses the aforementioned batch and scalability problem with the following distinguishing advantages: 1) high scalability and efficiency is achieved by using each shuffled node batch as a natural tuple – this choice also alleviates the need for explicit (and expensive) sampling; 2) enhanced and faster representations construction through graph filtering, which we show later increases *negative sample hardness*.

Specifically, **DMT** employs a GPR-based graph smoothing filter \mathcal{H} – as described earlier, the goal is to smooth node attributes \tilde{X} by graph structure via $\mathcal{X} = \mathcal{H}(\tilde{X}, A)$ such that each $x \in \mathcal{X}$ contains information from its neighborhood as well. The details of this filtering, and how it can be done on large graphs, is presented in the appendix. This approach can also help increase negative sample hardness, a property that has been shown to accelerate training and enhance the discriminative power [33,10,27] - details again are captured in the appendix.

DMT employs an extended version of the multi-class tuple loss from the deep metric learning [36]. Training is conducted in mini-batches and we consider each train batch \mathcal{X}_B of size \mathcal{B} as a \mathcal{B} -tuple $(x, \{x_i^+\}_{i=1}^m, \{x_i^-\}_{i=1}^q)$ with m positive samples x^+ and q negative samples x^- of x respectively (m and q are batch dependent). Furthermore, we define $h(x, x'; f) = \exp\{\frac{f(x)^T \cdot f(x')}{t}\}$, where we apply the cosine similarity as a metric distance such that each feature vector $f(x)$ is normalized before performing the Cartesian product. Temperature t is the radius of hypersphere where the representations lie [46] and can control penalty degree on hard negative samples as inspired by [45].

Now, the *multi-class tuple loss* function is:

$$L_{\text{DMT}}^{m,q}(x; f) = -\log \frac{h(x,x;f) + \sum_{i=1}^m h(x,x_i^+;f)}{h(x,x;f) + \sum_{i=1}^m h(x,x_i^+;f) + \sum_{i=1}^q h(x,x_i^-;f)} \quad (4)$$

Here, x is counted as one positive sample of itself to avoid zero-value inside the \log function. The loss function above shares a close mathematical form of supervised contrastive loss as proposed in [17] and enables us to create efficient mini-batch versions, while preserving the essential ideas behind metric or contrastive learning. One important aspect is because the function can work with varying m and q across batches, we can simply use all the positive and negative samples associated with any given batch.

3.3 DMAT-i Algorithm

In the unsupervised cases, $\{x_i^+\}$ and $\{x_i^-\}$ are no longer recognizable. To deal with this problem, we adopt the idea of contrastive learning, which includes multiple views of graph embeddings through *augmentation*, while assuming that the labeling still exists initially (thus, drawing from the deep metric learning framework). Then, we will show we can drop out the labels of the loss, which leads to the format of the contrastive learning loss.

Specifically, for one batch of samples \mathcal{X}_B of size \mathcal{B} together with their augmented counterparts, we have a $2\mathcal{B}$ -tuple $(x, \bar{x}, \{x_i^+\}_{i=1}^m, \{x_i^-\}_{i=1}^q)$ with m positive pairs and q negative pairs – here, \bar{x} denotes the augmented counterpart (trivial positive sample) of x . Thus, we introduce an immediate DMAT tuple loss $L_{\text{DMAT}}^{m,q}(x, \bar{x}; f)$ following the similar form of Eq.4:

$$L_{\text{DMAT}}^{\text{m,q}}(x, \bar{x}; f) = -\log \frac{h(x, \bar{x}; f) + \sum_{i=1}^m h(x, x_i^+; f)}{h(x, \bar{x}; f) + \sum_{i=1}^m h(x, x_i^+; f) + \sum_{i=1}^q h(x, x_i^-; f)} \quad (5)$$

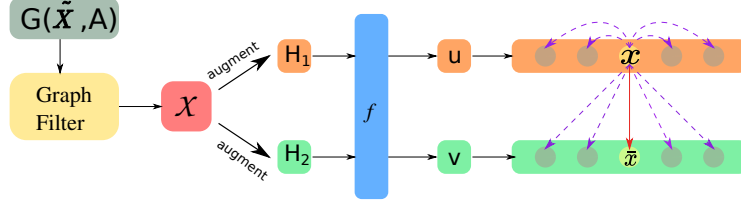


Fig. 1: Schematic of DMAT-i architecture. The graph filter generates smoothed node attributes \mathcal{X} by incorporating graph structural information. A pair of views (H_1, H_2) of \mathcal{X} are produced by augmentation and fed to the subsequent encoder f to generate latent representations $U = f(H_1)$ and $V = f(H_2)$. Metric distance measurement is performed on $U \cup V$. For each sample $x \in U$, its counterpart $\bar{x} \in V$ is the only recognizable positive sample.

Next, we extend DMAT to unsupervised cases where $\{x_i^+\}$ and $\{x_i^-\}$ are no longer recognizable. Here, the resulting method, DMAT-i, involves further simplification by extracting \bar{x} as the only positive sample of x while ignoring all other positive ones. The loss function is (mathematically equal to Eq.3):

$$L_{\text{DMAT-i}}^{\text{m,q}}(x, \bar{x}; f) = -\log \frac{h(x, \bar{x}; f)}{h(x, \bar{x}; f) + \sum_{i=1}^m h(x, x_i^+; f) + \sum_{i=1}^q h(x, x_i^-; f)} \quad (6)$$

Note $\{x_i^+\}_{i=1}^m$ and $\{x_i^-\}_{i=1}^q$ are explicitly denoted for ease of analysis, but they remain unknown during the training. Eq. 6 is in fact calculated without knowing any labels as:

$$L_{\text{DMAT-i}}^{\text{m,q}}(x, \bar{x}; f) = \log \left\{ \sum_{\substack{x' \in \mathcal{X}_B \\ x' \neq x}} h(x, x'; f) / h(x, \bar{x}; f) \right\}$$

Complete Algorithm: The general idea is illustrated in Figure 1. Augmented views are generated on the fly from \mathcal{X} by masking certain columns – the consequence is that the node features and structural information (encoded inside \mathcal{X}) are “distorted” simultaneously. A subsequent DNN based module can abstract information and perform metric similarity measurements (as in Eq. 6) between each pair of views. In real implementation, we use \mathcal{X} as the anchor view and each augmented view as the counterpart to calculate an average of training loss. Thus, the encoder will be optimized to learn robust characteristics of representations across different views. The overall objective to be maximized is defined as the average agreement $L_{\text{DMAT-i}}(x, \bar{x}; f)$ over all interchangeable view pairs as follows:

$$\mathbf{J} = \frac{1}{2\mathcal{B}} \sum_{x \in \mathcal{X}_B} [L_{\text{DMAT-i}}^{\text{m,q}}(x, \bar{x}; f) + L_{\text{DMAT-i}}^{\text{m,q}}(\bar{x}, x; f)] \quad (7)$$

The entire training process is presented in Algorithm 1. As input, \mathcal{X} is generated using random-walk based GnnBP (Graph neural network via Bidirectional Propagation [5]) as graph filtering. In line 3, multiple (n_{view}) augmented embedding will be generated from one batch of filtered feature \mathcal{X}_B by masking certain columns in \mathcal{X}_B . In line 5, the generated graph embedding views will be input into the DNN based encoder f to produce the latent representations. The deep metric learning in line 6 is performed in batches between encoded representations u of the anchor view \mathcal{X}_B and v of each augmented view H_B . The obtained embedding Z in line 8 will be used for the downstream learning tasks.

Algorithm 1 DMAT-i Training

Input data: GnnBP filtered attributes \mathcal{X} , Graph G , number of views: n_{view}

- 1: **for** $epoch = 1, 2, \dots$ **do**
- 2: **for** \mathcal{X}_B in \mathcal{X} **do**
- 3: Generate n_{view} augmented views of \mathcal{X}_B : $\{H_B\}$
- 4: **for** $i = 1, 2, \dots$ **do**
- 5: $u \leftarrow f(\mathcal{X}_B); v \leftarrow f(H_B^i)$
- 6: Compute multi-class triplet loss \mathbf{J} (Eq.7)
- 7: **end for**
- 8: SGD update on f to minimize \mathbf{J}
- 9: **end for**
- 10: **end for**
- 11: $Z \leftarrow f(\mathcal{X})$

4 Theoretical Analysis

DM(A)T and Contrastive Learning $\tilde{L}_{\text{Unbiased}}^{\mathcal{N}+1}(f)$ (Eq. 2) contrasts one positive sample against multiple negative samples and has been recognized as the ideal loss to optimize [8]. $L_{\text{DM(A)T}}^{\text{m,q}}(f)$ improves $\tilde{L}_{\text{Unbiased}}^{\mathcal{N}+1}(f)$ by recognizing multiple positive samples at the same time. It turns out that it can be shown as a lower bound of $L_{\text{Unbiased}}^{\mathcal{N}+1}(f)$, specifically:

Lemma 1 *For any embedding f , given the same size of tuples sharing one positive sample x_0^+ , i.e. $(x, x_0^+, \{x_i^-\}_{i=1}^{N-1})$ for $L_{\text{Unbiased}}^{\mathcal{N}+1}$ and $(x, x_0^+, \{x_i^+\}_{i=1}^m, \{x_i^-\}_{i=1}^q)$ for $L_{\text{DM(A)T}}^{\text{m,q}}$, we have: $L_{\text{DM(A)T}}^{\text{m,q}}(f) \leq \tilde{L}_{\text{Unbiased}}^{\mathcal{N}+1}(f)$*

Now, as we know, both $\tilde{L}_{\text{Unbiased}}^{\mathcal{N}+1}(f)$ and $L_{\text{DM(A)T}}^{\text{m,q}}(f)$ require p_x^+ and p_x^- , which can only be accessed from training data (i.e., during supervised learning). For unsupervised conditions, our $L_{\text{DMAT-i}}^{\text{m,q}}$ considers \bar{x} as the only available positive sample. Next, we will show how $L_{\text{DMAT-i}}^{\text{m,q}}$ contributes to a downstream learning task.

DMAT-i Generalization Bound on Node Classification We relate $L_{\text{DMAT-i}}^{\text{m,q}}$ to a supervised loss and present how $L_{\text{DMAT-i}}^{\text{m,q}}$ leads to a generalization bound for a supervised node classification task. Consider a supervised node classification task with K classes, we fix the embedding $f(\mathcal{X})$ from DMAT-i representation learning and train a linear classifier $\psi(\mathcal{X}) = f(\mathcal{X})W^\top$ with the standard multi-class softmax cross entropy loss $L_{\text{Softmax}}(\psi)$. We define the supervised loss for the representation $f(\mathcal{X})$ as: $L_{\text{Sup}}(f) = \inf_{W \in \mathbb{R}^{K \times d}} L_{\text{Softmax}}(fW^\top)$

[8] has proved $\tilde{L}_{\text{Unbiased}}^{\mathcal{N}+1}(f)$ as an upper bound of $L_{\text{Sup}}(f)$. What we contribute here is to bound the difference between $\tilde{L}_{\text{Unbiased}}^{\mathcal{N}+1}(f)$ and $L_{\text{DMAT-i}}^{\text{m,q}}$.

Theorem 1 *For any embedding f and same size of tuples,*

$$\left| \tilde{L}_{\text{Unbiased}}^{\mathcal{N}+1}(f) - L_{\text{DMAT-i}}^{\text{m,q}}(f) \right| \leq \sqrt{\frac{2(e^3 - e)(\tau^0)^2 \pi}{m}} + \sqrt{\frac{2(e^3 - e)(\tau^-)^2 \pi}{q}}$$

$$\tau^0 = \tau^+ \left(\frac{\left| \frac{1}{m} \sum_{i=1}^m h(x, x_i^+) - \mathbb{E}_{x^- \sim p_x^-} h(x, x^-) \right|}{\left| \frac{1}{m} \sum_{i=1}^m h(x, x_i^+) - \mathbb{E}_{x^+ \sim p_x^+} h(x, x^+) \right|} \right) \quad (8)$$

where $\sum_{i=1}^m h(x, x_i^+)$ represents the positive samples unrecognized by $L_{\text{DMAT-i}}^{\text{m,q}}$, i.e., *false negative samples*. Hence τ^0 covers the side effects from these false negatives and an empirical evaluation in appendix has shown reasonable small values of τ^0 for most samples across our experimental datasets.

In practice, we use an empirical estimate $\hat{L}_{\text{DMAT-i}}^{\text{m,q}}(f)$ over N data samples $x \in \mathcal{X}$, each sample with a tuple $(x, \bar{x}, \{x_i^+\}_{i=1}^m, \{x_i^-\}_{i=1}^q)$. The optimization process learns an empirical risk minimizer $\hat{f} \in \arg \min_{f \in \mathbb{F}} L_{\text{DMAT-i}}^{\text{m,q}}(f)$ from a function class \mathbb{F} . The generalization depends on the *empirical Rademacher complexity* $\mathcal{R}_{\mathcal{S}}(\mathbb{F})$ of \mathbb{F} with respect to our data sample $\mathcal{S} = \{x_j, \bar{x}_j, \{x_{i,j}^+\}_{i=1}^m, \{x_{i,j}^-\}_{i=1}^q\}_{j=1}^N$. Let $f|_{\mathcal{S}} = (f_k(x_j), f_k(\bar{x}_j), \{f_k(x_{i,j}^+)\}_{i=1}^m, \{f_k(x_{i,j}^-\}_{i=1}^q)_{j \in [N], k \in [d]} \in \mathbb{R}^{(m+q+2)dN}$ be the restriction of f onto \mathcal{S} , using $[N] = \{1, \dots, N\}$ and $[d] = \{1, \dots, d\}$. Then $\mathcal{R}_{\mathcal{S}}(\mathbb{F})$ is defined as: $\mathcal{R}_{\mathcal{S}}(\mathbb{F}) := \mathbb{E}_{\sigma} \sup_{f \in \mathbb{F}} \langle \sigma, f|_{\mathcal{S}} \rangle$ where $\sigma \sim \{\pm 1\}^{(m+q+1)dN}$ are *Rademacher random variables*. We provide a data dependent bound from $L_{\text{DMAT-i}}^{\text{m,q}}(f)$ on the downstream supervised generalization error as follows.

Theorem 2 *With probability at least $1 - \delta$, for all $f \in \mathbb{F}$ and $q \geq K - 1$,*

$$L_{\text{Sup}}(\hat{f}) \leq L_{\text{DMAT-i}}^{\text{m,q}}(f) + \mathcal{O} \left(\tau^0 \sqrt{\frac{1}{m}} + \tau^- \sqrt{\frac{1}{q}} + \frac{\lambda \mathcal{R}_{\mathcal{S}}(\mathbb{F})}{N} + \Gamma \sqrt{\frac{\log \frac{1}{\delta}}{N}} \right)$$

where $\lambda = \frac{(m+q)e}{m+q+e}$ and $\Gamma = \log(m+q)$.

The bound states that if the function class \mathbb{F} is sufficiently rich to contain embeddings for which $L_{\text{DMAT-i}}^{\text{m,q}}$ is small, then the representation encoder \hat{f} , learned from a large enough dataset, will perform well on the downstream classification task. The bound highlights the effects caused by the false negative pairs with the first term and also highlights the role of the inherent positive and negative sample sizes m and q per mini-batch in the objective function. The last term in the bound grows slowly with $m+q = 2\mathcal{B} - 2$, but the effect of this on the generalization error is small if the dataset size N is much larger than the batch size \mathcal{B} , as is common.

5 Experimental Results

Baselines: For the node clustering task, we compared the proposed DMAT-i model with multiple frameworks: 1) **KMeans** [13] (when applied to attributed graphs uses node attributes only); 2) **DeepWalk** [32], which uses topological information only, and seven recent frameworks that leverage both node attributes and graph structure: 3) **AGC (2019)**[54] that uses high-order graph convolution; 4) **DGI (2019)** [42] maximizes mutual information between patch representations and high-level summaries of graph; 5) **SDCN (2020)** [2] unifies an autoencoder module with a GCN module; 6) **AGE (2020)** [9] applies a customized Laplacian smoothing filter; 7) **SSGC (2021)** [57] is a variant of GCN that exploits a modified Markov Diffusion Kernel. 8) **GCA (2021)** [58] leverages a node-level contrastive loss between two augmented graph views to learn a graph representation; 9) **ProGCL (2022)** [49], on top of GCA, further proposed a more suitable measure for negatives hardness and similarity. To compare performance on node classification and link prediction, we select the most competitive graph embedding based frameworks correspondingly.

Scalability of Representation Construction As in Figure 2, all baselines hit specific ceilings as limited by the GPU memory capacity while DMAT-i can continuously scale with application of mini-batch training and use of random-walk to obtain approximate pagerank scores. Particularly, DMAT-i could handle 10^7 nodes, and no other frameworks could handle more than 10^6 nodes. The details of experimental settings are in appendix.

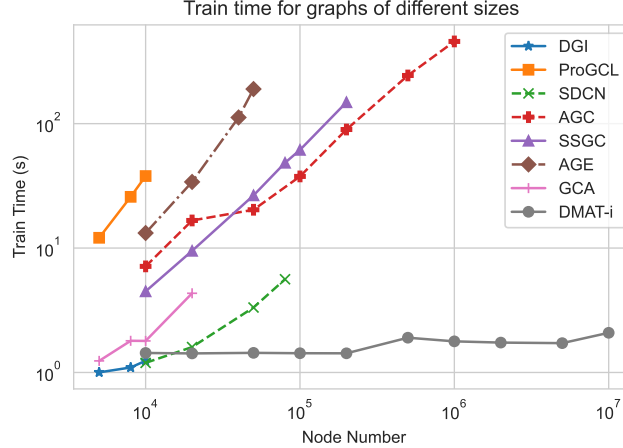


Fig. 2: Scalability of Different Frameworks: Training Time vs. No. of Nodes in Graph

5.1 Results on Downstream Tasks

DM(A)T is evaluated on performance of semi-supervised node classification while DMAT-i is evaluated for multiple tasks: node clustering, node classifi-

Table 1: Clustering performance on eight datasets (mean \pm std) where each experiment is performed for 10 runs. We employ six popular metrics: accuracy, Normalized Mutual Information (NMI), Average Rand Index (ARI), and macro F1-score are four metrics for ground-truth label analysis, whereas modularity [26] and conductance [51] are graph-level metrics. All metrics except conductance will indicate a better clustering output with a larger value. DMAT-i results highlighted in bold if they have the top 2 clustering performance. The asterisk indicates a convergence issue. Certain data points are missing when execution ran out of GPU memory. DGI can only handle five smaller datasets due to high GPU memory cost, and GCA also could not handle largest of these 8 datasets.

Dataset	Metric	KMeans	DeepWalk	SDCN	AGC	SSGC	AGE	DGI	GCA	ProGCL	DMAT-F
ACM	Accuracy \uparrow	66.62 \pm 0.55	50.59 \pm 4.27	89.63 \pm 0.31	78.21 \pm 0.00	84.43 \pm 0.29	90.18 \pm 0.13	90.17 \pm 0.28	89.91 \pm 0.46	89.18 \pm 1.70	91.60 \pm 0.70
	NMI \uparrow	32.41 \pm 0.34	16.12 \pm 4.96	66.74 \pm 0.75	46.31 \pm 0.01	56.15 \pm 0.51	66.92 \pm 0.30	67.84 \pm 0.72	66.58 \pm 0.91	64.64 \pm 3.04	70.95 \pm 1.44
	ARI \uparrow	30.22 \pm 0.41	18.56 \pm 5.80	72.00 \pm 0.75	48.02 \pm 0.00	60.17 \pm 0.60	73.12 \pm 0.31	73.28 \pm 0.66	72.49 \pm 1.08	70.72 \pm 3.88	76.72 \pm 1.75
	macro F1 \uparrow	66.83 \pm 0.57	46.56 \pm 4.43	89.60 \pm 0.32	78.26 \pm 0.00	84.44 \pm 0.29	90.18 \pm 0.13	90.12 \pm 0.27	89.89 \pm 0.46	89.16 \pm 1.71	91.59 \pm 0.70
	Modularity \uparrow	31.20 \pm 0.50	38.57 \pm 9.51	60.86 \pm 0.16	59.44 \pm 0.02	60.19 \pm 0.05	60.93 \pm 0.08	59.79 \pm 0.19	60.05 \pm 0.12	60.14 \pm 0.43	57.92 \pm 0.20
Conductance \downarrow	30.96 \pm 0.23	1.79 \pm 0.59	3.07 \pm 0.17	2.51 \pm 0.01	2.54 \pm 0.11	3.64 \pm 0.19	3.87 \pm 0.14	3.85 \pm 0.18	4.06 \pm 0.15	6.68 \pm 0.27	
DBLP	Accuracy \uparrow	38.65 \pm 0.58	38.99 \pm 0.02	69.08 \pm 1.95	69.06 \pm 0.06	68.66 \pm 1.95	*62.49 \pm 0.76	59.72 \pm 4.68	77.69 \pm 0.39	73.79 \pm 1.70	80.30 \pm 0.60
	NMI \uparrow	11.56 \pm 0.53	5.91 \pm 0.02	34.64 \pm 1.94	37.00 \pm 0.07	33.89 \pm 2.08	*37.32 \pm 0.50	26.90 \pm 4.43	46.24 \pm 0.57	41.54 \pm 1.27	51.00 \pm 0.81
	ARI \uparrow	6.95 \pm 0.39	5.83 \pm 0.02	36.31 \pm 2.86	33.69 \pm 0.13	37.30 \pm 3.13	*34.60 \pm 0.71	25.12 \pm 4.76	50.46 \pm 0.81	43.30 \pm 2.99	55.42 \pm 1.08
	macro F1 \uparrow	31.81 \pm 0.53	36.87 \pm 0.02	67.81 \pm 3.46	68.59 \pm 0.05	65.91 \pm 2.19	*59.16 \pm 0.83	59.31 \pm 4.69	77.29 \pm 0.37	72.96 \pm 2.03	79.94 \pm 0.59
	Modularity \uparrow	33.83 \pm 0.47	64.05 \pm 0.03	63.38 \pm 1.87	68.77 \pm 0.01	62.02 \pm 1.64	*48.62 \pm 0.87	50.16 \pm 3.77	63.01 \pm 0.28	64.62 \pm 1.02	55.67 \pm 0.71
Conductance \downarrow	36.20 \pm 0.51	4.03 \pm 0.02	7.56 \pm 0.54	5.29 \pm 0.01	3.24 \pm 0.52	*11.15 \pm 0.15	13.84 \pm 1.12	9.51 \pm 0.16	9.53 \pm 0.29	16.52 \pm 0.53	
Cora	Accuracy \uparrow	35.37 \pm 3.72	63.87 \pm 2.14	64.27 \pm 4.87	65.23 \pm 0.93	68.50 \pm 1.98	74.34 \pm 0.42	68.47 \pm 1.43	69.24 \pm 2.92	68.17 \pm 4.67	70.57 \pm 1.28
	NMI \uparrow	16.64 \pm 4.21	44.11 \pm 1.33	47.39 \pm 3.49	50.05 \pm 0.49	52.80 \pm 1.03	58.11 \pm 0.58	52.60 \pm 0.88	54.48 \pm 1.94	54.37 \pm 2.71	53.59 \pm 1.22
	ARI \uparrow	9.31 \pm 2.14	39.64 \pm 1.68	39.72 \pm 5.53	40.23 \pm 0.95	45.70 \pm 1.28	50.87 \pm 0.96	45.63 \pm 1.44	46.63 \pm 3.25	45.37 \pm 5.04	47.34 \pm 2.41
	macro F1 \uparrow	31.49 \pm 4.58	57.98 \pm 2.43	57.88 \pm 6.99	58.93 \pm 1.68	64.38 \pm 2.71	70.37 \pm 0.29	65.79 \pm 1.53	68.10 \pm 2.68	67.12 \pm 4.85	69.33 \pm 1.00
	Modularity \uparrow	20.77 \pm 3.37	72.98 \pm 0.79	62.59 \pm 5.18	69.98 \pm 0.46	73.71 \pm 0.45	71.89 \pm 0.14	69.86 \pm 0.29	74.18 \pm 0.51	74.36 \pm 0.38	74.19 \pm 0.39
Conductance \downarrow	59.77 \pm 5.31	7.88 \pm 0.35	18.32 \pm 2.26	11.08 \pm 1.61	9.41 \pm 0.55	8.23 \pm 0.11	13.64 \pm 0.69	10.27 \pm 0.31	9.47 \pm 0.54	10.04 \pm 0.52	
Citeseer	Accuracy \uparrow	46.70 \pm 4.33	43.56 \pm 1.03	63.42 \pm 3.31	67.18 \pm 0.52	67.86 \pm 0.26	66.06 \pm 0.78	68.68 \pm 0.76	66.23 \pm 1.00	66.43 \pm 1.16	67.46 \pm 0.41
	NMI \uparrow	18.42 \pm 3.26	16.02 \pm 0.56	37.28 \pm 2.19	41.37 \pm 0.70	41.86 \pm 0.22	40.56 \pm 0.88	43.22 \pm 0.91	40.81 \pm 1.15	41.41 \pm 1.03	41.75 \pm 0.62
	ARI \uparrow	18.42 \pm 3.26	16.37 \pm 0.66	37.40 \pm 2.79	42.10 \pm 0.87	42.95 \pm 0.30	39.84 \pm 0.75	44.53 \pm 1.02	41.24 \pm 1.45	41.73 \pm 1.52	42.48 \pm 0.60
	macro F1 \uparrow	44.47 \pm 4.44	40.37 \pm 0.97	56.16 \pm 4.53	62.68 \pm 0.48	63.61 \pm 0.23	60.80 \pm 0.75	64.41 \pm 0.70	62.16 \pm 0.95	62.53 \pm 1.11	62.83 \pm 0.38
	Modularity \uparrow	43.57 \pm 2.67	76.44 \pm 0.20	70.83 \pm 2.77	77.57 \pm 0.21	78.03 \pm 0.12	71.88 \pm 0.45	72.42 \pm 0.38	73.14 \pm 0.36	74.54 \pm 0.44	75.78 \pm 0.23
Conductance \downarrow	37.21 \pm 2.19	2.98 \pm 0.12	7.98 \pm 1.99	1.72 \pm 0.04	1.75 \pm 0.03	4.84 \pm 0.13	7.19 \pm 0.55	6.96 \pm 0.58	5.57 \pm 0.23	3.02 \pm 0.22	
Pubmed	Accuracy \uparrow	59.50 \pm 0.02	69.98 \pm 0.04	59.95 \pm 1.00	61.54 \pm 0.00	70.71 \pm 0.00	69.66 \pm 0.09	-	64.10 \pm 2.11	-	70.90 \pm 0.20
	NMI \uparrow	31.21 \pm 0.10	29.09 \pm 0.11	17.78 \pm 0.91	29.11 \pm 0.00	32.12 \pm 0.00	29.06 \pm 0.16	-	28.50 \pm 2.41	-	32.49 \pm 0.28
	ARI \uparrow	28.08 \pm 0.08	31.81 \pm 0.13	16.39 \pm 1.16	26.16 \pm 0.00	33.26 \pm 0.00	31.26 \pm 0.12	-	26.15 \pm 2.46	-	33.52 \pm 0.36
	macro F1 \uparrow	58.15 \pm 0.02	68.51 \pm 0.06	60.29 \pm 1.02	60.28 \pm 0.00	69.91 \pm 0.00	68.68 \pm 0.08	-	63.69 \pm 2.34	-	70.10 \pm 0.20
	Modularity \uparrow	34.92 \pm 0.06	57.25 \pm 0.26	55.53 \pm 0.86	50.40 \pm 0.00	57.73 \pm 1.35	57.48 \pm 0.10	-	53.90 \pm 1.76	-	57.56 \pm 0.44
Conductance \downarrow	17.27 \pm 0.04	4.67 \pm 0.03	7.50 \pm 0.58	8.65 \pm 0.00	3.93 \pm 0.00	4.75 \pm 0.16	-	9.51 \pm 0.80	-	4.10 \pm 0.22	
Amazon Photo	Accuracy \uparrow	27.86 \pm 0.81	77.27 \pm 2.48	60.42 \pm 3.36	55.93 \pm 0.09	56.16 \pm 1.05	66.96 \pm 3.00	61.05 \pm 2.48	77.21 \pm 0.72	78.27 \pm 0.97	76.53 \pm 1.32
	NMI \uparrow	13.78 \pm 1.19	68.97 \pm 1.96	50.08 \pm 3.28	53.35 \pm 0.05	51.74 \pm 1.66	56.73 \pm 2.62	52.93 \pm 2.11	66.48 \pm 1.23	70.11 \pm 1.32	66.94 \pm 1.37
	ARI \uparrow	5.62 \pm 0.42	58.64 \pm 2.81	40.08 \pm 3.95	25.31 \pm 0.10	33.86 \pm 1.36	46.48 \pm 3.37	39.59 \pm 2.74	56.09 \pm 0.92	61.30 \pm 1.71	58.84 \pm 1.07
	macro F1 \uparrow	23.78 \pm 0.48	71.59 \pm 2.47	53.13 \pm 5.99	51.56 \pm 0.06	52.00 \pm 0.67	62.13 \pm 3.33	59.60 \pm 2.94	76.23 \pm 0.71	72.35 \pm 1.49	70.05 \pm 0.77
	Modularity \uparrow	8.38 \pm 0.51	73.18 \pm 0.12	59.25 \pm 4.04	57.69 \pm 0.04	62.07 \pm 1.88	64.07 \pm 1.45	61.12 \pm 1.39	67.76 \pm 0.83	70.81 \pm 0.47	70.72 \pm 0.19
Conductance \downarrow	76.38 \pm 0.58	8.47 \pm 0.23	20.17 \pm 3.88	4.42 \pm 0.00	8.37 \pm 2.15	15.81 \pm 1.49	22.14 \pm 1.65	15.27 \pm 1.11	10.46 \pm 0.72	10.98 \pm 0.67	
Coauthor CS	Accuracy \uparrow	27.96 \pm 1.09	67.10 \pm 2.98	56.86 \pm 3.40	62.24 \pm 1.81	66.19 \pm 1.19	76.35 \pm 3.14	-	72.02 \pm 2.54	-	76.92 \pm 1.26
	NMI \uparrow	15.42 \pm 2.25	66.67 \pm 0.86	54.79 \pm 2.44	65.22 \pm 0.44	70.06 \pm 0.67	76.75 \pm 1.66	-	73.95 \pm 1.02	-	72.55 \pm 0.41
	ARI \uparrow	1.02 \pm 0.74	53.66 \pm 2.91	40.41 \pm 4.52	46.96 \pm 3.54	58.50 \pm 0.17	71.27 \pm 5.46	-	63.92 \pm 3.21	-	66.91 \pm 1.38
	macro F1 \uparrow	11.68 \pm 1.56	63.36 \pm 2.84	29.36 \pm 3.22	51.42 \pm 1.27	60.17 \pm 1.94	71.10 \pm 1.96	-	63.63 \pm 3.28	-	70.48 \pm 3.13
	Modularity \uparrow	9.61 \pm 1.88	72.88 \pm 0.41	53.05 \pm 2.02	69.58 \pm 0.14	71.82 \pm 0.14	70.45 \pm 1.71	-	69.91 \pm 0.58	-	69.79 \pm 0.40
Conductance \downarrow	37.12 \pm 4.10	17.09 \pm 0.66	*23.09 \pm 1.89	19.80 \pm 0.24	19.76 \pm 0.22	14.41 \pm 0.32	-	21.96 \pm 0.60	-	21.13 \pm 0.66	
Coauthor PHY	Accuracy \uparrow	56.19 \pm 0.75	87.97 \pm 0.01	64.65 \pm 6.92	77.41 \pm 0.00	55.70 \pm 2.26	92.04 \pm 0.06	-	-	-	89.30 \pm 0.70
	NMI \uparrow	11.72 \pm 1.92	69.13 \pm 0.02	50.60 \pm 3.71	62.11 \pm 0.02	57.71 \pm 1.31	75.84 \pm 0.13	-	-	-	72.54 \pm 0.80
	ARI \uparrow	8.25 \pm 1.26	79.15 \pm 0.03	48.76 \pm 9.58	72.43 \pm 0.02	44.91 \pm 1.58	84.44 \pm 0.16	-	-	-	77.68 \pm 1.61
	macro F1 \uparrow	24.74 \pm 2.11	83.32 \pm 0.02	48.51 \pm 4.68	62.09 \pm 0.00	55.26 \pm 2.30	88.90 \pm 0.08	-	-	-	86.65 \pm 0.91
	Modularity \uparrow	5.74 \pm 0.83	47.96 \pm 0.00	44.97 \pm 3.16	45.31 \pm 0.00	60.70 \pm 0.39	47.69 \pm 0.07	-	-	-	50.56 \pm 0.27
Conductance \downarrow	10.56 \pm 1.47	5.99 \pm 0.00	19.86 \pm 7.16	5.80 \pm 0.00	13.47 \pm 0.07	5.73 \pm 0.03	-	-	-	7.31 \pm 0.31	

Table 2: Accuracy for semi-supervised node classification task with different data usage for embedding generation: 1) using 10% of data with labels; 2) using all data without labels.

Data Usage	Method	Cora	Citeseer	Pubmed	ACM	DBLP	Amazon Photo	Coauthor CS	Coauthor PHY
train data (labeled)	DMT	84.30 \pm 0.25	70.42 \pm 0.33	86.46 \pm 0.16	91.42 \pm 0.36	77.59 \pm 0.30	92.60 \pm 0.42	93.30 \pm 0.12	95.44 \pm 0.03
	DMAT	83.92 \pm 0.45	71.39 \pm						

cation, and link prediction. Our framework is compared with existing state-of-the-art approaches on 8 real-world datasets (with details in appendix).

Node Clustering We set the number of clusters to the number of ground-truth classes and perform K-Means algorithm [13] on resulting embedding Z from DMAT-i following previous efforts [31,2,57,9]. Table 1 summarizes clustering results. DMAT-i maintains either the state-of-the-art clustering results or is fairly close to the best. In particular, DMAT-i further reduced state-of-the-art accuracy gap between unsupervised learning and transductive supervised learning as presented later in Table 2 across datasets such as DBLP and Coauthor PHY. Not surprisingly, deep clustering methods that use both node attributes and graph structure appear to be more robust and stronger than those using either of them (KMeans and DeepWalk), although the latter shows good performance for certain datasets. Compared with GCN based methods like SDCN, DMAT-i shows significant performance gain due to solving over-smoothing issues through graph filtering. For clustering methods like AGC, SSGC or AGE with carefully designed Laplacian-smoothing filters, DMAT-i can still outperform them in most cases. The most competitive clustering performance comes from AGE on several datasets – however, it does not even converge for DBLP. DMAT-i achieves robust convergence across all real-word datasets – a detailed summary of convergence time across different datasets is presented in the appendix.

Table 3: Link prediction performance.

Dataset	Metrics	DMAT-i	SSGC	AGE	GCA	ProGCL
Cora	AP	92.41 ± 0.28	93.24 ± 0.00	92.26 ± 0.30	92.95 ± 0.41	92.87 ± 0.28
	AUC	92.62 ± 0.29	92.14 ± 0.00	92.07 ± 0.21	92.95 ± 0.34	93.60 ± 0.13
Citeseer	AP	95.52 ± 0.26	96.14 ± 0.00	92.22 ± 0.48	93.38 ± 0.39	95.65 ± 0.28
	AUC	95.19 ± 0.26	95.29 ± 0.00	92.66 ± 0.44	92.57 ± 0.49	95.59 ± 0.24
Pubmed	AP	95.42 ± 0.08	97.53 ± 0.00	84.67 ± 0.09	92.65 ± 0.44	-
	AUC	95.18 ± 0.10	97.84 ± 0.00	86.70 ± 0.12	93.81 ± 0.37	-
ACM	AP	97.55 ± 0.17	82.33 ± 0.00	98.14 ± 0.10	92.61 ± 1.05	97.02 ± 0.23
	AUC	97.41 ± 0.17	81.15 ± 0.00	97.51 ± 0.18	94.19 ± 0.75	97.31 ± 0.18
DBLP	AP	95.50 ± 0.37	95.88 ± 0.00	92.68 ± 0.31	93.41 ± 0.61	95.99 ± 0.24
	AUC	95.50 ± 0.50	95.22 ± 0.00	90.96 ± 0.43	92.47 ± 0.59	95.38 ± 0.23
Amazon Photo	AP	92.73 ± 0.23	83.93 ± 0.00	91.65 ± 0.23	76.26 ± 1.39	93.43 ± 0.65
	AUC	93.89 ± 0.20	89.21 ± 0.00	93.12 ± 0.19	81.28 ± 1.34	95.66 ± 0.42
Coauthor CS	AP	94.76 ± 0.14	88.96 ± 0.00	93.96 ± 0.18	82.70 ± 0.98	-
	AUC	95.03 ± 0.12	93.56 ± 0.00	93.61 ± 0.15	83.54 ± 0.74	-
Coauthor PHY	AP	91.25 ± 0.20	93.92 ± 0.00	94.35 ± 0.08	-	-
	AUC	92.75 ± 0.15	96.57 ± 0.00	95.20 ± 0.06	-	-

Node Classification For the transductive semi-supervised node classification task, we applied train-validation-test data split with fraction as train (10%), validation (10%), and test (80%). Following the experimental settings of SSGC [57] and GCA [58], we evaluate the classification performance of DM(A)T and DMAT-i by using a linear classifier to perform semi-supervised classification and report the accuracy. As shown in Table 2, the embedding generation methods are categorized based on the availability of labels, where DM(A)T learns from train data (10% of all data) with labels and DMAT-i can proceed in an unsupervised way on all data samples. For comparison, we apply DMAT-i in both settings.

With labelled training data, DM(A)T turns out to achieve high quality of representations and shows superior results. DMAT-i, however, fails to recognize part of positive samples as compared with DMAT in this condition and lose some accuracy. When labels are completely unavailable, we can see that competitive results have been observed from DMAT-i compared to other advanced baselines under unsupervised setting. More importantly, DMAT-i generally achieves better performance when generating embedding in unsupervised condition than “partially-supervised” condition (with partial labels available). That is because much more samples i.e. all data, are included during triplet loss optimization.

Link Prediction To evaluate DMAT-i on this task, we remove 5% edges for validation and 10% edges for test while keeping all node attributes [38,31,9]. The reconstructed adjacency matrix \hat{A} can be calculated as per the previous publication [38]: $\hat{A}=\sigma(ZZ^T)$, where σ denotes the sigmoid function. For comparison purposes, we report area under the ROC curve (AUC) and average precision (AP) following settings from previous works [38,31,9]. As shown in Table 3, DMAT-i is robust, i.e, produces high-quality link prediction (above 90% for both metrics for all datasets), whereas no other methods has a comparable consistency.

6 Conclusions

This paper has presented a scalable graph (node-level) learning framework. Employing a mutli-class triplet loss function, we have introduced both semi-supervised learning and unsupervised algorithms. We have also established connections between triplet loss and contrastive loss functions and also theoretically shown how our method leads to generalization error bound on the downstream classification task. The learned representation is used for three downstream tasks: node clustering, classification, and link prediction. Our extensive evaluation has shown better scalability over any existing method, and consistently high accuracy (state-of-the-art or very competitive in each case).

A Proofs for Theoretical Analysis

A.1 Assumptions and Notations

The underlying set of discrete latent classes are denoted as $\mathcal{C}(\cdot)$ representing semantic content and the distribution over classes as $\rho(y)$, i.e. probability of observing class y . Given a pair of sample vectors (x, x') from $\mathcal{X} \in \mathbb{R}^{N \times d}$, $p_x^+(x') = p(x'|C(x') = C(x))$ is the probability of observing x' as a positive sample for x and $p_x^-(x') = p(x'|C(x') \neq C(x))$ the probability of a negative one. Assume that the class probabilities $\rho(y) = \tau^+$ are uniform, i.e. the fraction of each class in each tuple stays constant. τ^+ of each class can be empirically calculated as the fraction of each class in the whole dataset. The data distribution can be decomposed as:

$$p(x') = \tau^+ p_x^+(x') + \tau^- p_x^-(x')$$

We define $h(x, x'; f) = \exp\{\frac{f(x)^T \cdot f(x')}{t}\}$. For simplicity of analysis, we assume $t = 1$ yielding $h(x, x'; f) = \exp\{f(x)^T \cdot f(x')\}$

A.2 Proof of Lemma 1

Lemma 1 For any embedding f , given the same size of tuples sharing one positive sample x_0^+ , i.e. $(x, x_0^+, \{x_i^-\}_{i=1}^{N-1})$ for $L_{\text{Unbiased}}^{N+1}$ and $(x, x_0^+, \{x_i^+\}_{i=1}^m, \{x_i^-\}_{i=1}^q)$ for $L_{\text{DM(A)T}}^{m,q}$, we have:

$$L_{\text{DM(A)T}}^{m,q}(f) \leq \tilde{L}_{\text{Unbiased}}^{N+1}(f)$$

Proof (Proof of Lemma 1).

We first focus on the DMAT loss. Consider the DMAT tuple $(x, x_0^+, \{x_i^+\}_{i=1}^m, \{x_i^-\}_{i=1}^q)$ with a fixed size $(N+1)$, we have $N+1 = 2 + m + q$, i.e. $N-1 = m + q$

$L_{\text{DMAT}}^{m,q}(f)$ is the empirical estimate of $\tilde{L}_{\text{DMAT}}^{m,q}(f)$ as follows:

$$\tilde{L}_{\text{DMAT}}^{m,q}(f) = -\log \frac{h(x, x_0^+) + m\mathbb{E}_{x^+ \sim p_x^+} h(x, x^+)}{h(x, x_0^+) + m\mathbb{E}_{x^+ \sim p_x^+} h(x, x^+) + q\mathbb{E}_{x^- \sim p_x^-} h(x, x^-)}$$

In comparison with $\tilde{L}_{\text{Unbiased}}^{N+1}$ [8] on the tuple $(x, x_0^+, \{x_i^-\}_{i=1}^{N-1})$:

$$\begin{aligned} \tilde{L}_{\text{Unbiased}}^{N+1}(f) &= -\log \frac{h(x, x_0^+)}{h(x, x_0^+) + (N-1)\mathbb{E}_{x^- \sim P_x^-} h(x, x^-)} \\ &= -\log \frac{h(x, x_0^+)}{h(x, x_0^+) + (m+q)\mathbb{E}_{x^- \sim P_x^-} h(x, x^-)} \end{aligned}$$

Then we have:

$$\tilde{L}_{\text{DMAT}}^{m,q}(f) \leq -\log \frac{h(x, x_0^+)}{h(x, x_0^+) + q\mathbb{E}_{x^- \sim P_x^-} h(x, x^-)} \leq \tilde{L}_{\text{Unbiased}}^{N+1}(f)$$

The first inequality is based on the fact that $\frac{a+c}{b+c} \geq \frac{a}{b}$ for $a \leq b$ and $a, b, c \geq 0$ and the second inequality is due to $m \geq 0$.

For $L_{\text{DMT}}^{m,q}(f)$ on the tuple $(x, x_0^+, \{x_i^+\}_{i=1}^m, \{x_i^-\}_{i=1}^q)$, $L_{\text{DMT}}^{m,q}(f)$ is the empirical estimate of $\tilde{L}_{\text{DMT}}^{m,q}(f)$ as follows:

$$\tilde{L}_{\text{DMT}}^{m,q}(f) = -\log \frac{h(x, x) + h(x, x_0^+) + m\mathbb{E}_{x^+ \sim p_x^+} h(x, x^+)}{h(x, x) + h(x, x_0^+) + m\mathbb{E}_{x^+ \sim p_x^+} h(x, x^+) + q\mathbb{E}_{x^- \sim p_x^-} h(x, x^-)}$$

The only difference between $\tilde{L}_{\text{DMT}}^{m,q}(f)$ and $\tilde{L}_{\text{DMAT}}^{m,q}(f)$ is that $\tilde{L}_{\text{DMT}}^{m,q}(f)$ includes an additional term $h(x, x)$. All the proof above for $L_{\text{DMAT}}^{m,q}$ still holds for $L_{\text{DMT}}^{m,q}$.

A.3 Proof of Theorem 1

We follow a similar proof strategy in [8]. To prove Theorem 1, we first seek a bound on the tail probability that the difference between the integrands of two objective functions $\tilde{L}_{\text{DMAT-}i}^{\text{m,q}}(f)$ and $\tilde{L}_{\text{Unbiased}}^{\mathcal{N}+1}(f)$ given the same size of tuples is greater than a specific threshold ε :

$$\begin{aligned} \mathbb{P}(\Delta \geq \varepsilon), \quad \Delta &= \left| L_{\text{DMAT-}i}^{\text{m,q}}(f) - \tilde{L}_{\text{Unbiased}}^{\mathcal{N}+1}(f) \right| \\ &= \left| -\log \frac{h(x, \bar{x})}{h(x, \bar{x}) + \sum_{i=1}^m h(x, x_i^+) + \sum_{i=1}^q h(x, x_i^-)} \right. \\ &\quad \left. + \log \frac{h(x, \bar{x})}{h(x, \bar{x}) + (m+q)\mathbb{E}_{x^- \sim p_x^-} h(x, x^-)} \right| \end{aligned}$$

where Δ depends on x, \bar{x} and the collections of samples $\{x_i^+\}_{i=1}^m$ and $\{x_i^-\}_{i=1}^q$. Here we apply $\mathcal{N} - 1 = m + q$ as from *Proof of Lemma 1*. This tail will be controlled by the following lemma.

Lemma A.1 *With x and \bar{x} in \tilde{X} fixed, let $\{x_i^+\}_{i=1}^m$ and $\{x_i^-\}_{i=1}^q$ be collections of i.i.d. random variables sampled from p_x^+ and p_x^- respectively. Then $\forall \varepsilon > 0$,*

$$\mathbb{P}(\Delta \geq \varepsilon) \leq 2 \exp\left(-\frac{m\varepsilon^2}{2(e^3 - e)(\tau^0)^2}\right) + 2 \exp\left(-\frac{q\varepsilon^2}{2(e^3 - e)(\tau^-)^2}\right)$$

where

$$\tau^0 = \tau^+ \left(\frac{\left| \frac{1}{m} \sum_{i=1}^m h(x, x_i^+) - \mathbb{E}_{x^- \sim p_x^-} h(x, x^-) \right|}{\left| \frac{1}{m} \sum_{i=1}^m h(x, x_i^+) - \mathbb{E}_{x^+ \sim p_x^+} h(x, x^+) \right|} \right)$$

Proof (Proof of Lemma A.1).

First, we define $g(x, \{x_i^+\}_{i=1}^m, \{x_i^-\}_{i=1}^q)$ as:

$$g(x, \{x_i^+\}_{i=1}^m, \{x_i^-\}_{i=1}^q) = \frac{1}{m+q} \left(\sum_{i=1}^m h(x, x_i^+) + \sum_{i=1}^q h(x, x_i^-) \right)$$

$$\begin{aligned}
\mathbb{P}(\Delta \geq \varepsilon) &= \mathbb{P}\left(\left|\log \{h(x, \bar{x}) + (m+q)g(x, \{x_i^+\}_{i=1}^m, \{x_i^-\}_{i=1}^q)\} \right. \right. \\
&\quad \left. \left. - \log \{h(x, \bar{x}) + (m+q)\mathbb{E}_{x^- \sim p_x^-} h(x, x^-)\} \right| \geq \varepsilon\right) \\
&= \mathbb{P}\left(\log \{h(x, \bar{x}) + (m+q)g(x, \{x_i^+\}_{i=1}^m, \{x_i^-\}_{i=1}^q)\} \right. \\
&\quad \left. - \log \{h(x, \bar{x}) + (m+q)\mathbb{E}_{x^- \sim p_x^-} h(x, x^-)\} \geq \varepsilon\right) \\
&\quad + \mathbb{P}\left(-\log \{h(x, \bar{x}) + (m+q)g(x, \{x_i^+\}_{i=1}^m, \{x_i^-\}_{i=1}^q)\} \right. \\
&\quad \left. + \log \{h(x, \bar{x}) + (m+q)\mathbb{E}_{x^- \sim p_x^-} h(x, x^-)\} \geq \varepsilon\right) \\
&= \mathbb{P}_1(\varepsilon) + \mathbb{P}_2(\varepsilon)
\end{aligned}$$

The first term can be bounded as:

$$\begin{aligned}
\mathbb{P}_1(\varepsilon) &= \mathbb{P}\left(\log \frac{h(x, \bar{x}) + (m+q)g(x, \{x_i^+\}_{i=1}^m, \{x_i^-\}_{i=1}^q)}{h(x, \bar{x}) + (m+q)\mathbb{E}_{x^- \sim p_x^-} h(x, x^-)} \geq \varepsilon\right) \\
&\leq \mathbb{P}\left(\frac{(m+q)g(x, \{x_i^+\}_{i=1}^m, \{x_i^-\}_{i=1}^q) - (m+q)\mathbb{E}_{x^- \sim p_x^-} h(x, x^-)}{h(x, \bar{x}) + (m+q)\mathbb{E}_{x^- \sim p_x^-} h(x, x^-)} \geq \varepsilon\right) \\
&= \mathbb{P}\left(g(x, \{x_i^+\}_{i=1}^m, \{x_i^-\}_{i=1}^q) - \mathbb{E}_{x^- \sim p_x^-} h(x, x^-) \geq \right. \tag{9} \\
&\quad \left. \varepsilon \left\{ \frac{1}{m+q} h(x, \bar{x}) + \mathbb{E}_{x^- \sim p_x^-} h(x, x^-) \right\} \right) \\
&\leq \mathbb{P}\left(g(x, \{x_i^+\}_{i=1}^m, \{x_i^-\}_{i=1}^q) - \mathbb{E}_{x^- \sim p_x^-} h(x, x^-) \geq \varepsilon e^{-1}\right). \tag{10}
\end{aligned}$$

The first inequality follows by applying the fact that $\log x \leq x - 1$ for $x > 0$. The second inequality holds since $\frac{1}{m+q}h(x, \bar{x}) + \mathbb{E}_{x^- \sim p_x^-} h(x, x^-) \geq e^{-1}$. Similarly, the second term can be bounded as:

$$\begin{aligned}
\mathbb{P}_2(\varepsilon) &= \mathbb{P}\left(\log \frac{h(x, \bar{x}) + (m+q)\mathbb{E}_{x^- \sim p_x^-} h(x, x^-)}{h(x, \bar{x}) + (m+q)g(x, \{x_i^+\}_{i=1}^m, \{x_i^-\}_{i=1}^q)} \geq \varepsilon\right) \\
&\leq \mathbb{P}\left(\frac{(m+q)\mathbb{E}_{x^- \sim p_x^-} h(x, x^-) - (m+q)g(x, \{x_i^+\}_{i=1}^m, \{x_i^-\}_{i=1}^q)}{h(x, \bar{x}) + (m+q)g(x, \{x_i^+\}_{i=1}^m, \{x_i^-\}_{i=1}^q)} \geq \varepsilon\right) \\
&= \mathbb{P}\left(\mathbb{E}_{x^- \sim p_x^-} h(x, x^-) - g(x, \{x_i^+\}_{i=1}^m, \{x_i^-\}_{i=1}^q) \geq \varepsilon \left(\frac{1}{m+q} h(x, \bar{x}) + g(x, \{x_i^+\}_{i=1}^m, \{x_i^-\}_{i=1}^q)\right)\right) \quad (11) \\
&\leq \mathbb{P}\left(\mathbb{E}_{x^- \sim p_x^-} h(x, x^-) - g(x, \{x_i^+\}_{i=1}^m, \{x_i^-\}_{i=1}^q) \geq \varepsilon e^{-1}\right). \quad (12)
\end{aligned}$$

Combining Eq.(10) and Eq.(12), we have

$$\mathbb{P}(\Delta \geq \varepsilon) \leq \mathbb{P}\left(\left|g(x, \{x_i^+\}_{i=1}^m, \{x_i^-\}_{i=1}^q) - \mathbb{E}_{x^- \sim p_x^-} h(x, x^-)\right| \geq \varepsilon e^{-1}\right)$$

$$\begin{aligned}
&\left|g(x, \{x_i^+\}_{i=1}^m, \{x_i^-\}_{i=1}^q) - \mathbb{E}_{x^- \sim p_x^-} h(x, x^-)\right| \\
&= \left|\frac{1}{m+q} \left(\sum_{i=1}^m h(x, x_i^+) + \sum_{i=1}^q h(x, x_i^-)\right) - \mathbb{E}_{x^- \sim p_x^-} h(x, x^-)\right| \\
&= \left|\frac{m}{m+q} \frac{1}{m} \sum_{i=1}^m h(x, x_i^+) + \frac{q}{m+q} \frac{1}{q} \sum_{i=1}^q h(x, x_i^-) - (\tau^+ + \tau^-) \mathbb{E}_{x^- \sim p_x^-} h(x, x^-)\right| \\
&= \left|\tau^+ \left(\frac{1}{m} \sum_{i=1}^m h(x, x_i^+) - \mathbb{E}_{x^+ \sim p_x^+} h(x, x^+)\right) + \tau^- \left(\frac{1}{q} \sum_{i=1}^q h(x, x_i^-) - \mathbb{E}_{x^- \sim p_x^-} h(x, x^-)\right)\right| \\
&\leq \tau^+ \left|\frac{1}{m} \sum_{i=1}^m h(x, x_i^+) - \mathbb{E}_{x^+ \sim p_x^+} h(x, x^+)\right| + \tau^- \left|\frac{1}{q} \sum_{i=1}^q h(x, x_i^-) - \mathbb{E}_{x^- \sim p_x^-} h(x, x^-)\right| \\
&= \tau^0 \left|\frac{1}{m} \sum_{i=1}^m h(x, x_i^+) - \mathbb{E}_{x^+ \sim p_x^+} h(x, x^+)\right| + \tau^- \left|\frac{1}{q} \sum_{i=1}^q h(x, x_i^-) - \mathbb{E}_{x^- \sim p_x^-} h(x, x^-)\right|
\end{aligned}$$

where

$$\tau^0 = \tau^+ \left(\frac{\left|\frac{1}{m} \sum_{i=1}^m h(x, x_i^+) - \mathbb{E}_{x^+ \sim p_x^+} h(x, x^+)\right|}{\left|\frac{1}{m} \sum_{i=1}^m h(x, x_i^+) - \mathbb{E}_{x^+ \sim p_x^+} h(x, x^+)\right|}\right)$$

Here $\frac{m}{m+q} \simeq \tau^+$ and $\frac{q}{m+q} \simeq \tau^-$ are based on the assumption of uniform class distribution, i.e. the fraction of each class stays constant in each tuple: $\rho(y) = \tau^+$. Further, we have:

$$\begin{aligned}
& \mathbb{P}\left(\left|g(x, \{x_i^+\}_{i=1}^m, \{x_i^-\}_{i=1}^q) - \mathbb{E}_{x^- \sim p_x^-} h(x, x^-)\right| \geq \varepsilon e^{-1}\right) \\
& \leq \mathbb{P}\left(\tau^0 \left|\frac{1}{m} \sum_{i=1}^m h(x, x_i^+) - \mathbb{E}_{x^+ \sim p_x^+} h(x, x^+)\right|\right. \\
& \quad \left. + \tau^- \left|\frac{1}{q} \sum_{i=1}^q h(x, x_i^-) - \mathbb{E}_{x^- \sim p_x^-} h(x, x^-)\right| \geq \varepsilon e^{-1}\right) \\
& \leq \text{I}(\varepsilon) + \text{II}(\varepsilon).
\end{aligned}$$

where

$$\begin{aligned}
\text{I}(\varepsilon) &= \mathbb{P}\left(\tau^0 \left|\frac{1}{m} \sum_{i=1}^m h(x, x_i^+) - \mathbb{E}_{x^+ \sim p_x^+} h(x, x^+)\right| \geq \frac{\varepsilon e^{-1}}{2}\right) \\
\text{II}(\varepsilon) &= \mathbb{P}\left(\tau^- \left|\frac{1}{q} \sum_{i=1}^q h(x, x_i^-) - \mathbb{E}_{x^- \sim p_x^-} h(x, x^-)\right| \geq \frac{\varepsilon e^{-1}}{2}\right).
\end{aligned}$$

Hoeffding's inequality states that if X, X_1, \dots, X_N are i.i.d random variables bounded in the range $[a, b]$:

$$\mathbb{P}\left(\left|\frac{1}{n} \sum_{i=1}^N X_i - \mathbb{E}X\right| \geq \varepsilon\right) \leq 2 \exp\left(-\frac{2N\varepsilon^2}{b-a}\right)$$

With $e^{-1} \leq h(x, \bar{x}) \leq e$ in our case, then:

$$\text{I}(\varepsilon) \leq 2 \exp\left(-\frac{m\varepsilon^2}{2(e^3 - e)(\tau^0)^2}\right) \quad \text{and} \quad \text{II}(\varepsilon) \leq 2 \exp\left(-\frac{q\varepsilon^2}{2(e^3 - e)(\tau^-)^2}\right)$$

With Lemma A.1 at hand, we are ready to prove Theorem 1.

Theorem 1 *For any embedding f and same size of tuples, we have:*

$$\left|\tilde{L}_{\text{Unbiased}}^{\mathcal{N}+1}(f) - L_{\text{DMAT-i}}^{\text{m,q}}(f)\right| \leq \sqrt{\frac{2(e^3 - e)(\tau^0)^2\pi}{m}} + \sqrt{\frac{2(e^3 - e)(\tau^-)^2\pi}{q}}$$

Proof. By Jensen's inequality, we can push the absolute value inside the expectation to see that $|\tilde{L}_{\text{Unbiased}}^{\mathcal{N}+1}(f) - L_{\text{DMAT-i}}^{\text{m,q}}(f)| \leq \mathbb{E}\Delta$. Further, we write the expectation of Δ for fixed x, \bar{x} as the integral of its tail probability,

$$\begin{aligned}
\mathbb{E} \Delta &= \mathbb{E}_{x, \bar{x}} [\mathbb{E}[\Delta | x, \bar{x}]] = \mathbb{E}_{x, \bar{x}} \left[\int_0^\infty \mathbb{P}(\Delta \geq \varepsilon | x, \bar{x}) d\varepsilon \right] \\
&\leq \int_0^\infty 2 \exp\left(-\frac{m\varepsilon^2}{2(e^3 - e)(\tau^0)^2}\right) d\varepsilon + \int_0^\infty 2 \exp\left(-\frac{q\varepsilon^2}{2(e^3 - e)(\tau^-)^2}\right) d\varepsilon \\
&= \sqrt{\frac{2(e^3 - e)(\tau^0)^2\pi}{m}} + \sqrt{\frac{2(e^3 - e)(\tau^-)^2\pi}{q}}
\end{aligned}$$

Since the tail probably bound of Theorem A.1 holds uniformly for all fixed x, \bar{x} , the outer expectation can be removed [8]. Both integrals in the final step can be computed via:

$$\int_0^\infty e^{-cz^2} dz = \frac{1}{2} \sqrt{\frac{\pi}{c}}.$$

A.4 Proof of Theorem 2

Theorem 2 aims to derive a data dependent bound from $L_{\text{DMAT-i}}^{m,q}(f)$ on the downstream supervised generalization error $L_{\text{Sup}}(f)$. To prove Theorem 2, we need to employ Lemma A.2, Lemma A.3 and Lemma A.4 provided as follows.

For one batch of samples \mathcal{X}_B of size B together with their augmented counterparts, we have a $2B$ -tuple $(x, \bar{x}, \{x_i^+\}_{i=1}^m, \{x_i^-\}_{i=1}^q)$ with \bar{x} as the augmented counterpart (a trivial positive sample) of x . $\{x_i^+\}$ are m positive samples other than \bar{x} and $\{x_i^-\}$ are q negative samples. Rewrite $L_{\text{DMAT-i}}^{m,q}(f)$ as:

$$\begin{aligned} L_{\text{DMAT-i}}^{m,q}(f) &= -\log \left\{ \frac{e^{f(x)^\top f(\bar{x})}}{e^{f(x)^\top f(\bar{x})} + \sum_{i=1}^m e^{f(x)^\top f(x_i^+)} + \sum_{i=1}^q e^{f(x)^\top f(x_i^-)}} \right\} \\ &= \log \left\{ 1 + \sum_{i=1}^m e^{f(x)^\top (f(x_i^+) - f(\bar{x}))} + \sum_{i=1}^q e^{f(x)^\top (f(x_i^-) - f(\bar{x}))} \right\} \\ &= \ell \left(\{f(x)^\top (f(x_i^+) - f(\bar{x}))\}_{i=1}^m, \{f(x)^\top (f(x_i^-) - f(\bar{x}))\}_{i=1}^q \right) \end{aligned}$$

For simplicity, we denote the loss as:

$$\ell(\{a_i\}_{i=1}^m, \{b_i\}_{i=1}^q) = \log \left\{ 1 + \sum_{i=1}^m a_i + \sum_{i=1}^q b_i \right\}.$$

where

$$a_i = e^{f(x)^\top (f(x_i^+) - f(\bar{x}))} \quad \text{and} \quad b_i = e^{f(x)^\top (f(x_i^-) - f(\bar{x}))}$$

To derive our bound, we will exploit a concentration of measure result due to [1]. They consider an unsupervised loss of the form

$$L_{un}(f) = \mathbb{E} \left[\ell(\{f(x)^\top (f(x_i^-) - f(x^+))\}_{i=1}^k) \right],$$

where $(x, x^+, x_1^-, \dots, x_k^-)$ are sampled from any fixed distribution on \mathcal{X}^{k+2} with x^+, x_i^- representing positive and negative sample of x respectively (they were particularly focused on the case where $x_i^- \sim p$, but the proof holds for arbitrary distributions [8]). Let \mathbb{F} be a class of representation functions $\mathcal{X} \rightarrow \mathbb{R}^d$ such that $\|f(\cdot)\| \leq R$ for $R > 0$. The corresponding empirical risk minimizer is:

$$\hat{f} \in \arg \min_{f \in \mathbb{F}} \frac{1}{N} \sum_{j=1}^N \ell(\{f(x_j)^\top (f(x_{j_i}^-) - f(x_j^+))\}_{i=1}^k)$$

over a training set $\mathcal{S} = \{(x_j, x_j^+, x_{j_1}^-, \dots, x_{j_k}^-)\}_{j=1}^N$ of i.i.d. samples. Their result bounds the loss of the empirical risk minimizer as follows.

Lemma A.2 [1] *Let $\ell : \mathbb{R}^k \rightarrow \mathbb{R}$ be η -Lipschitz and bounded by Γ . Then with probability at least $1 - \delta$ over the training set $\mathcal{S} = \{(x_j, x_j^+, x_{j_1}^-, \dots, x_{j_k}^-)\}_{j=1}^N$, for all $f \in \mathbb{F}$*

$$L_{un}(\hat{f}) \leq L_{un}(f) + \mathcal{O} \left(\frac{\eta R \sqrt{k} \mathcal{R}_{\mathcal{S}}(\mathbb{F})}{N} + \Gamma \sqrt{\frac{\log \frac{1}{\delta}}{N}} \right)$$

where

$$\mathcal{R}_{\mathcal{S}}(\mathbb{F}) = \mathbb{E}_{\sigma \sim \{\pm 1\}^{(k+2)dN}} \left[\sup_{f \in \mathbb{F}} \langle \sigma, f|_{\mathcal{S}} \rangle \right],$$

$$\text{and } f|_{\mathcal{S}} = \left(f_t(x_j), f_t(x_j^+), f_t(x_{j_1}^-), \dots, f_t(x_{j_k}^-) \right)_{\substack{j \in [N] \\ t \in [d]}}.$$

In our particular case, f are normalized embeddings with $\|f(\cdot)\| \leq 1$ and thus $e^{-1} \leq a_i, b_i \leq e$. We have $k = m + q$ and $R = 1$. So, it remains to obtain constants η and Γ such that $\ell(\{a_i\}_{i=1}^m, \{b_i\}_{i=1}^q)$ is η -Lipschitz, and bounded by Γ .

Lemma A.3 *With $e^{-1} \leq a_i, b_i \leq e$, the function $\ell(\{a_i\}_{i=1}^m, \{b_i\}_{i=1}^q)$ is η -Lipschitz, and bounded by Γ for*

$$\eta = \frac{e\sqrt{m+q}}{m+q+e}, \quad \Gamma = \mathcal{O}(\log(m+q)).$$

Proof. First, it is easily observed that ℓ is upper bounded by plugging in $a_i = b_i = e$ yielding a bound of

$$\log \left\{ 1 + \sum_{i=1}^m e + \sum_{i=1}^q e \right\} = \mathcal{O}(\log(m+q))$$

To bound the Lipschitz constant we view ℓ as a composition $\ell(\{a_i\}_{i=1}^m, \{b_i\}_{i=1}^q) = \phi(g(\{a_i\}_{i=1}^m, \{b_i\}_{i=1}^q))$

$$\phi(z) = \log(1+z)$$

$$z = g(\{a_i\}_{i=1}^m, \{b_i\}_{i=1}^q) = \sum_{i=1}^m a_i + \sum_{i=1}^q b_i$$

where $(m+q)e^{-1} \leq z \leq (m+q)e$ and thus $\partial_z \phi(z) = \frac{1}{1+z} \leq \frac{e}{m+q+e}$. We therefore conclude that ϕ is $\frac{e}{m+q+e}$ -Lipschitz. The Lipschitz constant of g is bounded by the Forbenius norm of the Jacobian of g , which equals

$$\sqrt{\sum_{i=1}^m \left(\frac{\partial g}{\partial a_i}\right)^2 + \sum_{i=1}^q \left(\frac{\partial g}{\partial b_i}\right)^2} = \sqrt{m+q}$$

Lemma A.4 [8] *For any embedding f for a downstream K -way classification, whenever $N \geq K$ we have*

$$L_{\text{Sup}}(f) \leq \tilde{L}_{\text{Unbiased}}^{N+1}(f).$$

Here, we change notation of $L_{\text{Unbiased}}^N(f)$ from [8] into $L_{\text{Unbiased}}^{N+1}(f)$ for consistency in our work. The number of negative samples is $N-1$, requiring $N-1 \geq K-1$ as in [8] yields $N \geq K$. Now we have all the requested lemmas, together with Theorem 1 we are ready to prove Theorem 2 as follows.

Theorem 2 *With probability at least $1 - \delta$, for all $f \in \mathbb{F}$ and $q \geq K - 1$,*

$$L_{\text{Sup}}(\hat{f}) \leq L_{\text{DMAT-i}}^{\text{m,q}}(f) + \mathcal{O}\left(\tau^0 \sqrt{\frac{1}{m}} + \tau^- \sqrt{\frac{1}{q}} + \frac{\lambda \mathcal{R}_{\mathcal{S}}(\mathbb{F})}{N} + \Gamma \sqrt{\frac{\log \frac{1}{\delta}}{N}}\right)$$

where $\lambda = \eta \sqrt{k} = \frac{(m+q)e}{m+q+e}$ and $\Gamma = \log(m+q)$.

Proof. By Lemma A.4 and Theorem 1, requiring the number of negative samples $q \geq K - 1$, we have

$$L_{\text{sup}}(\hat{f}) \leq L_{\text{DMAT-i}}^{\text{m,q}}(\hat{f}) + \sqrt{\frac{2(e^3 - e)(\tau^0)^2 \pi}{m}} + \sqrt{\frac{2(e^3 - e)(\tau^-)^2 \pi}{q}}$$

As shown earlier, our unsupervised loss $L_{\text{DMAT-i}}^{\text{m,q}}(f)$ follows the same form of $L_{\text{un}}(f)$ as in Lemma A.2. Combining Lemma A.2 and Lemma A.3, with probability at least $1 - \delta$, for all $f \in \mathbb{F}$, we have:

$$L_{\text{DMAT-i}}^{\text{m,q}}(\hat{f}) \leq L_{\text{DMAT-i}}^{\text{m,q}}(f) + \mathcal{O}\left(\frac{\lambda \mathcal{R}_{\mathcal{S}}(\mathbb{F})}{N} + \Gamma \sqrt{\frac{\log \frac{1}{\delta}}{N}}\right),$$

where $\lambda = \eta \sqrt{k} = \frac{(m+q)e}{m+q+e}$ and $\Gamma = \log(m+q)$.

B Additional Results

B.1 T-SNE from DMAT-i node clustering on Cora Dataset

Figure 3 intuitively shows comparison between node embeddings using t-SNE algorithm [41]. We can see that the graph filter and encoder module can gradually recognize node semantic distribution with less overlapping areas.

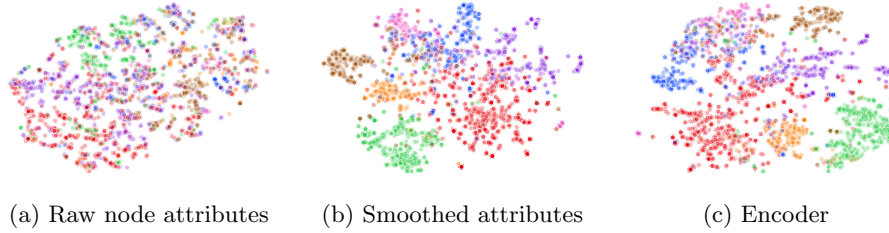


Fig. 3: Cora t-SNE for different embeddings. Each color represents a distinct class.

B.2 DMAT-i Training Process and Convergence Time

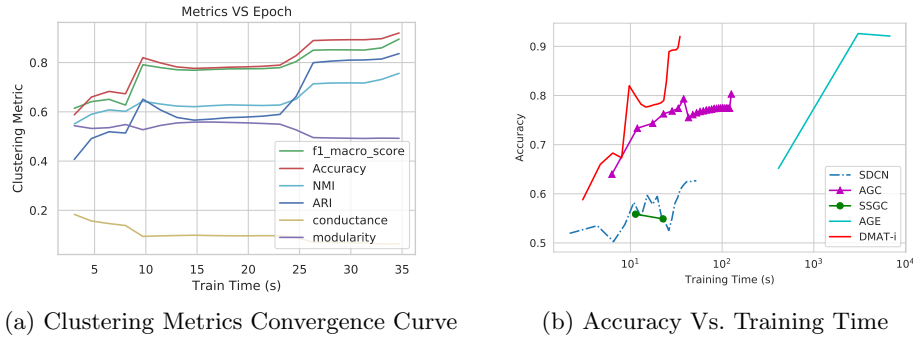


Fig. 4: DMAT-i Training Process on Coauthor PHY

DMAT-i achieves robust convergence across all real-word datasets – Figure 4a shows the training process of DMAT-i on Coauthor PHY with all metrics converged to a steady state and detailed comparison of accuracy and training time for different methods on this dataset is shown in Figure 4b. GCA and DGI are not shown because they could not even execute with this dataset. Overall,

Table 4: Convergence time (s) comparison. The asterisk indicates a convergence issue with stop time reported.

Dataset	ACM	DBLP	Cora	Citeseer	Pubmed	Coauthor PHY	Coauthor CS	Amazon	Photo
SDCN	3.74 ± 0.52	3.37 ± 0.52	6.52 ± 0.73	5.18 ± 1.16	23.29 ± 0.62	52.20 ± 0.15	22.78 ± 0.70	11.67 ± 0.84	
ProGCL	29.87 ± 2.50	65.99 ± 1.48	17.99 ± 1.42	35.72 ± 1.72	-	-	-	293.36 ± 16.79	
AGC	1.75 ± 0.20	0.57 ± 0.22	0.82 ± 0.28	7.49 ± 1.10	0.94 ± 0.22	125.44 ± 0.83	17.78 ± 0.64	3.43 ± 0.57	
SSGC	5.83 ± 0.94	1.92 ± 0.74	2.18 ± 1.88	22.24 ± 3.87	26.29 ± 0.31	23.65 ± 0.73	37.31 ± 14.69	6.53 ± 3.12	
AGE	95.61 ± 0.16	*88.57 ± 0.80	70.36 ± 0.34	182.10 ± 0.52	1343.35 ± 40.15	6799.57 ± 33.19	463.10 ± 1.89	87.15 ± 1.11	
DGI	15.01 ± 0.70	16.18 ± 0.63	13.64 ± 0.91	15.22 ± 0.62	-	-	-	13.12 ± 0.45	
GCA	8.09 ± 0.64	11.27 ± 2.34	7.43 ± 0.57	8.65 ± 0.56	74.76 ± 2.81	-	144.71 ± 0.74	47.24 ± 3.06	
DMAT-i	10.15 ± 0.85	16.04 ± 0.70	3.06 ± 0.71	14.25 ± 1.13	3.26 ± 0.37	33.86 ± 1.35	37.41 ± 1.99	17.49 ± 2.71	

we can see that DMAT-i obtains best accuracy, while converging in much less time compared with the most competitive baseline AGE.

A detailed summary of convergence time across different datasets is presented in Table 4. One observation we can make is that GCA becomes several times more expensive than DMAT-i for all the datasets with 15,000 or more edges (and cannot be executed for Coauthor PHY). AGE is significantly more expensive, whereas other methods that are faster do not produce results of the same quality.

B.3 Empirical evaluation of τ^0

From Eq.8, we empirically evaluate $\mathbb{E}_{x^- \sim p_x^-} h(x, x^-)$ by $\widehat{\mathbb{E}}_{x^- \in \mathcal{X}} h(x, x^-)$, i.e. the average of all negative samples of each sample x across all samples \mathcal{X} . Similar empirical approximation $\widehat{\mathbb{E}}_{x^+ \in \mathcal{X}} h(x, x^+)$ will be applied to $\mathbb{E}_{x^+ \sim p_x^+} h(x, x^+)$. An empirical evaluation of τ^0 across 8 datasets is provided in Figure 5. The values of τ^0 remain small values for most samples as in Table 5.

Table 5: DMAT-i empirical evaluation of τ^0 distribution with several quantiles: Q1 (25%) and Q3 (75%)

Quantile	Coauthor	CS	Coauthor	PHY	Amazon	Photo	ACM	Citeseer	DBLP	Cora	Pubmed
Q1		1.90		1.48		1.26	5.76	1.91	2.38	1.06	3.52
Median		5.11		6.21		2.74	11.67	4.09	4.50	2.32	8.09
Q3		16.18		16.35		5.70	25.47	9.14	9.47	5.88	18.37

B.4 Empirical Evaluation of representation Negative Hardness

Our train objectives of DM(A)T and DMAT-i are hardness-aware loss functions with the strength of penalties on hard negative samples [45]. In supervised machine learning, using hard (true negative) samples can accelerate a learning method by correcting mistakes faster. In representation learning, we consider a pair of negative examples as being informative if their latent representation are mapped nearby but should be actually be far apart.

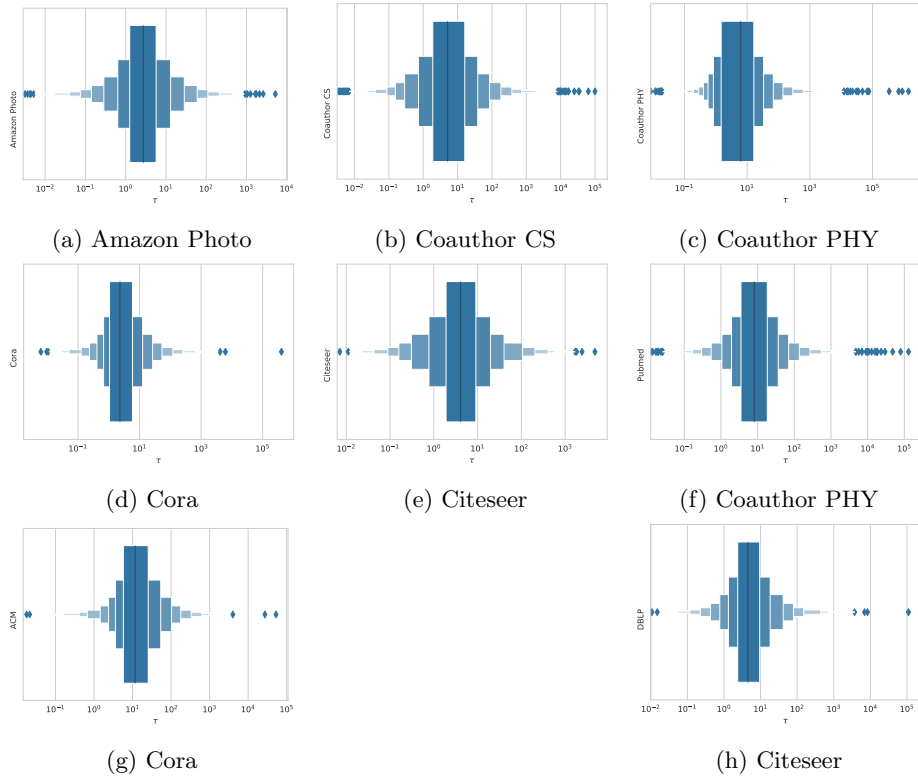


Fig. 5: Empirical evaluation of τ^0 distribution across 8 datasets.

To investigate the hardness-awareness of DMAT-i, we studied the distribution of similarity scores $Z_i^T Z_j$ as in Algorithm 1 among negative sample pairs. The idea is that a negative sample pair with a higher score will be more difficult to discriminate and thus considered to be hard. Hard negative samples have been proven to accelerate the learning process, while too much hardness can also degrade the performance.

We perform an empirical evaluation of negative hardness in 7 out of 8 datasets (except Amazon PHY whose large size makes such evaluation unfeasible). As shown in **Figure 6**, the smoothed features contain many more hard negative sample pairs than raw features. For most datasets, the hardness concentrates more within a range of similarity scores $[0.25, 0.50]$, therefore more hard negative samples with *mild hardness* are included due to graph filtering. The embedding after training process shows a significant reduction of hardness, which indicates that our model is able to discriminate most of the negative pairs through continuous self-optimization.

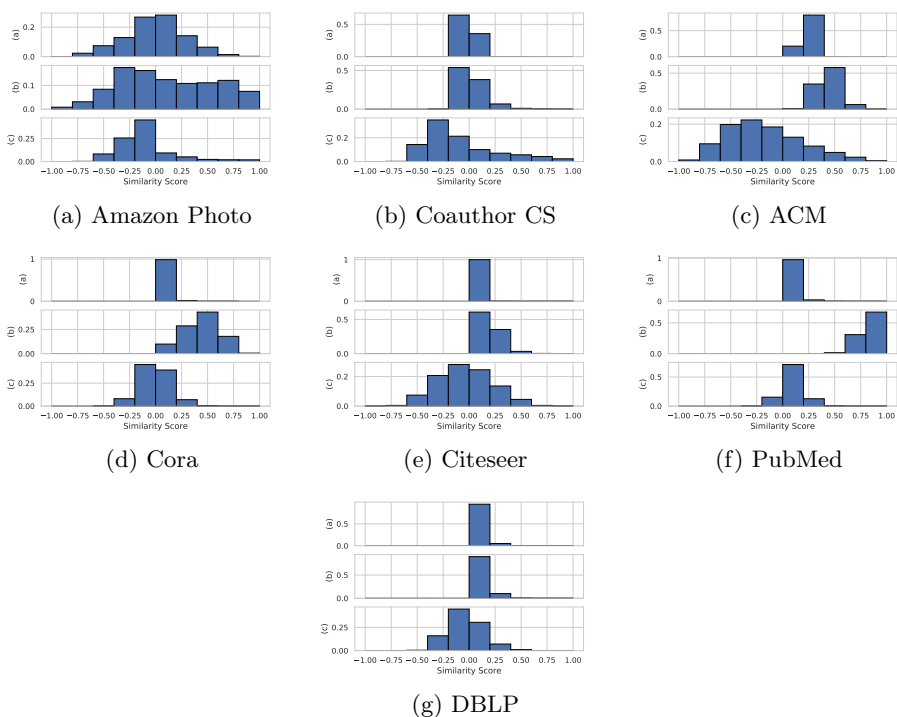


Fig. 6: Hard negative sample pair fraction distribution across 7 datasets. (a) raw node attributes; (b) smoothed features; (c) embedding after training

C Generalized PageRank and Laplacian Smoothing Filters

We present how \mathcal{X} is calculated for the purpose of our approach. As a background, Graph convolutional Network (GCN) has been a popular technique for incorporating graph structure information for representation learning. However, it has been shown to suffer from over-smoothing issues, leading to degraded learning performance [21]. As a remedy for such issue, graph smoothing filters have been successful, with specific instances being Adaptive Graph Convolution (AGC) [54], Simple Spectral Graph Convolution (SSGC) [57] and Adaptive Graph Encoder (AGE) [9]. We observe that Laplacian smoothing can be approximated by Generalized Page Rank (GPR), which can be computed by a scalable and parallelizable random-walk based algorithm [5].

Returning to the notation introduced at the beginning of the section, let D be the diagonal degree matrix and the graph Laplacian matrix is defined as $L = D - A$. Let $\tilde{A} = A + I_N$ and \tilde{D} represent the augmented adjacency matrix with self-loops added and the corresponding diagonal degree matrix. With $\tilde{L} = \tilde{D} - \tilde{A}$ as the Laplacian matrix corresponding to \tilde{A} , the generalized Laplacian smoothing filter \mathcal{H} [37] used by Cui *et al.* [9] can be stated as:

$$\hat{Y} = \mathcal{H}\tilde{X} = (I - \gamma\tilde{D}^{-\frac{1}{2}}\tilde{L}\tilde{D}^{-\frac{1}{2}})\tilde{X} \quad (13)$$

Now, stacking L Laplacian smoothing filters from Eq.13 yields:

$$\hat{Y} = \mathcal{H}^L\tilde{X} = (\gamma\tilde{D}^{-\frac{1}{2}}\tilde{A}\tilde{D}^{-\frac{1}{2}} + (1 - \gamma)I_n)^L \cdot \tilde{X} \quad (14)$$

While Laplacian smoothing can serve as a filter that addressed over-smoothing issues of GCN, GPR provides a mechanism to perform scalable computations. To this end, Chen *et al.* [5] designed a localized bidirectional propagation algorithm as an unbiased estimate of the Generalized PageRank matrix (P) [20] as below:

$$P = \sum_{l=0}^L w_l T^l = \sum_{l=0}^L w_l (\tilde{D}^{r-1} \tilde{A} \tilde{D}^r)^l \cdot \tilde{X} \quad (15)$$

with $r \in [0, 1]$ as the convolution coefficient, w_l 's as the weights of different order convolution matrices satisfying $\sum_{l=0}^{\infty} w_l \leq 1$ and $T^l = (\tilde{D}^{r-1} \tilde{A} \tilde{D}^r)^l \cdot X$ as the l -th step propagation matrix.

Eq. 14 can be generalized into GPR in Eq.15 by setting $r = 0.5$ and manipulating the weights w_l to simulate various diffusion processes. Therefore, we use the parallelizable bidirection propagation algorithm from Chen *et al.* [5] as a highly scalable graph smoothing filter to ease the downstream tasks. By setting $w_l = \alpha(1 - \alpha)^l$ with α as the teleport probability [18], we focused on one setup where \mathbf{P} becomes the PPR (Personalized PageRank) as used in APPNP

[18]. The hyper-parameter α will adjust the size of the neighborhood for node information aggregation [18] such that we can balance the needs of preserving locality and leveraging information of nodes from further distances. PPR can avoid over-smoothing issues even when aggregating attributes from infinite layers of neighboring nodes [18].

D Complexity Analysis

Table 6: Time and Space complexity during Training on the GPU $O(\cdot)$, with N as the number of nodes, E as the number of edges, d as the feature dimension, L as the number of neural network layers, \mathcal{B} as the batch size.

Complexity	GCA [58]	DGI [42]	SDCN [2]	ProGCL [49]	AGC [54]	SSGC [57]	AGE [9]	DM(A)T
Computation Cost	$L \cdot E \cdot d + L \cdot N \cdot d^2$	$L \cdot E \cdot d + L \cdot N \cdot d^2$	$L \cdot E \cdot d + L \cdot N \cdot d^2$	$L \cdot E \cdot d + L \cdot N \cdot d^2$	$E \cdot d + N \cdot d$	$E \cdot d + N \cdot d$	$E \cdot d + N \cdot d$	$L \cdot \mathcal{B} \cdot d^2$
Memory Cost	$N \cdot d + E + L \cdot d^2$	$N \cdot d + E + L \cdot d^2$	$N \cdot d + E + L \cdot d^2$	$N \cdot d + E + L \cdot d^2$	$N \cdot d + E$	$N \cdot d + E$	$N \cdot d + E$	$\mathcal{B} \cdot d + L \cdot d^2$

For this analysis, let N be the number of nodes, L be the number of neural network layers, E be the total number of edges, d be the number of features and \mathcal{B} be the batch size. For simplicity, we assume number of features for all layers is fixed as d . In Table 6, for DM(A)T, the computational cost is $O(L \cdot \mathcal{B} \cdot d^2 + N \cdot d)$. Here, $O(L \cdot \mathcal{B} \cdot d^2)$ corresponds to L layers of matrix multiplication for DNN module during the training. The memory cost is $O(\mathcal{B} \cdot d + L \cdot d^2) - \mathcal{B} \cdot d$ relates to saving a batch of input \mathcal{X} and $L \cdot d^2$ is for storing model learning parameters $\{W^{(l)}\}_{l=1}^L$.

In contrast, all the other baseline clustering frameworks include an expensive sparse matrix-matrix multiplication $\tilde{A} \cdot \tilde{X}$, where \tilde{A} refers to the adjacency matrix of the entire graph and \tilde{X} is the feature matrix. GCA, DGI, SDCN and ProGCL frameworks use a traditional GCN module, so, they have an identical complexity, which turns out to be most expensive. AGC, SSGC, AGE are similar – the computational cost is $O(E \cdot d + N \cdot d)$ since each $\tilde{T} \cdot \tilde{X}$ costs $E \cdot d$ and $N \cdot d$ is the cost of summation over filters and adding features. For all these three frameworks, the memory cost is $O(N \cdot d + E)$. Overall, since $E \gg N \gg d$ and the batch size \mathcal{B} can be defined by users based on resource availability, the training process of our framework can be easily fit onto GPU memory for large-scale graphs.

E Related Work

Attributed Graph Representation Learning. Graph Autoencoder (GAE) based models [38,30,44] learn node embeddings that can recover either node features or the adjacency matrix. Adaptive Graph Convolution (AGC) [54] uses high-order graph convolution to capture global cluster structure and adaptively selects the appropriate order for different graphs. Simple Spectral Graph Convolution (SSGC) [57] is a variant of GCN that exploits a modified Markov Diffusion

Kernel. Adaptive Graph Encoder (AGE) [9] combines a customized Laplacian smoothing filter with an adaptive encoder to strengthen the filtered features for better node embeddings. In using GCN modules for node clustering, SDCN [2] is a self-supervised method. [55] proposed a graph debiased contrastive learning approach to jointly perform representation learning and clustering. GCA [58] is a graph contrastive representation learning method with adaptive augmentation. ProGCL [49] boosts the graph contrastive learning by estimating the probability of a negative being true. DCRN [22] improves the representation discriminative capability for node clustering by reducing information correlation.

Deep Metric Learning. [3] laid the foundation of this area motivated by signature verification. [7] discriminatively trains the network for face verification via contrastive loss, [33] learns a unified embedding for face clustering and recognition through triplet loss, and [10] focuses on visual categorization. [36] proposed (N+1)-tuple loss for a variety of visual recognition tasks. [53] proposes a supervised distance metric learning for graph classification. It should be noted that the contrastive loss here aims to ensure that the distance between examples from different classes is larger than a certain margin [36]. The methods we next discuss under contrastive learning have a different emphasis.

Contrastive Learning. As one major branch of self-supervised learning, contrastive learning, when combined with augmentation techniques, has achieved state-of-the-art performance in visual representation learning tasks [29,15,40,6,48]. This idea has also been applied for node-level representation learning for graph-structured data [42,58]. Deep Graph Infomax (DGI) [42] achieves advanced node classification performance by extending a contrastive learning mechanism (from precursor work Deep InfoMax [15]). GCA [58] applied the contrastive loss from [6] to maximize agreements at the node level and performed well on node classification tasks. We later discuss how our approach differs and also perform extensive experimental comparison.

F Details for Experimental Setup

Our DM(A)T framework is implemented in PyTorch 1.7 on CUDA 10.1, whereas the graph filtering procedure is in C++. Our experiments are performed on nodes with a dual Intel Xeon 6148s @2.4GHz CPU and dual NVIDIA Volta V100 w/ 16GB memory GPU and 384 GB DDR4 memory. Graph filtering is executed on CPU while tuple loss based training process is performed on a single GPU. We applied a AdamW optimization method with a decoupled weight decay regularization technique [23].

F.1 Datasets Details

As in Table 7 **ACM** [2] is a paper network from ACM – nodes correspond to paper, edges represent common author, features are bag-of-words of keywords, and the class labels are the research areas. **DBLP** [2] is an author network – nodes represent authors, edges represent co-authorship, features are the bag-of-words

Table 7: Datasets Statistics

dataset	Nodes	Classes	Features	Edges
ACM	3025	3	1870	13,128
DBLP	4058	4	334	3528
Citeseer	3327	6	3703	4732
Cora	2708	7	1433	5429
Pubmed	19717	3	500	44,338
Amazon Photo	7650	8	745	71,831
Coauthor CS	18333	15	6805	81,894
Coauthor PHY	34493	5	8415	247,962

of keywords, and class labels are the author’s research fields based on the conferences they submitted papers to. **Amazon Photo** [24] is a segment of Amazon co-purchase graph – nodes are goods, edges indicate two goods are frequently bought together, features are bag-of-words from product reviews and class labels represent product categories. We also include three Citation Networks[34], i.e., **Cora**, **Pubmed** and **Citeseer** here, the nodes correspond to papers, edges are citation links, features are bag-of-word of abstracts, and labels are paper topics. For consistent comparison, we use these datasets without row-normalization as described in [39]. We include two Microsoft Co-authorship datasets [35], which are **Coauthor CS** and **Coauthor PHY**, based on Microsoft Academic Graph for computer science and physics, respectively – here, nodes represent authors, edges represent co-authorship, features are paper keywords, and class labels indicate the most common fields of study.

F.2 Scalability of Representation Construction settings

Synthetic datasets were used to evaluate scalability of DMAT-i and other frameworks. We used PaRMAT [16] to generate undirected synthetic graphs of growing size with edge count set as 20 times the number of nodes and a random feature matrix with a dimension of 1000. For each clustering method, we performed 5-epoch training, repeated each experiment 5 times, and report average times.

F.3 DMAT Hyper-parameter Settings

Detailed hyper-parameters settings are included in Table 8. `Learning_rate` corresponds to the learning rates during DNN based encoder training with a contrastive loss. During the augmentation of node embeddings to produce multiple views, `mask_fraction` is the portion of columns to mask and `view_num` is the number of generated views. τ is the temperature parameter of contrastive loss [58]. And `n_epochs` is the number of iterations for DNN training. The architecture describes the number of neurons on each layer of the encoder. We applied a decoupled weight decay regularization [23] resulting in the factor `weight_decay`. The size of batch during mini-batch training is controlled by `batch_size`. The last

Table 8: DMAT hyper-parameter settings on 8 datasets

Hyper-parameters	ACM	DBLP	Cora	CiteSeer	PubMed	Amazon	Photo	Coauthor CS	Coauthor PHY
learning_rate	$1e-3$	$1e-3$	$1e-4$	$1e-4$	$1e-5$		$8e-5$	$1e-5$	$2e-5$
architecture	256-128	256-256	256-128	256-512	256-256		512-512	256-512	256-512
τ	2.0	2.0	1.0	4.0	0.8		2.0	1.2	0.5
n_epochs	400	300	300	400	200		500	400	400
mask_fraction	0.6	0.2	0.08	0.2	0.2		0.1	0.4	0.1
view_num	4	4	3	4	2		4	5	5
weight_decay	0.02	0.05	0.02	0.05	0.05		0.1	0.05	0.05
batch_size	512	512	512	512	512		256	512	512
α	0.4	0.6	0.1	0.4	0.01		0.03	0.1	0.08
r_{max}	$1e-5$	$1e-4$	$1e-6$	$1e-5$	$1e-5$		$1e-6$	$1e-5$	$1e-5$
rrz	0.4	0.5	0.4	0.4	0.4		0.5	0.4	0.4

three parameters are from GnnBP framework [5], $\alpha \in (0, 1)$ is teleport probability defined in Personalized PageRank weights ($w_l = \alpha(1 - \alpha)^l$); r_{max} is the threshold during reverse push propagation from the feature vectors; rrz is the convolutional coefficient.

F.4 Baseline Justification and Source Codes

In justifying our choice of baselines for the node clustering task, we observe that methods that utilize both node features and graph structure achieve a significant improvement over other approaches that only exploit one of them. Earlier attributed graph embedding frameworks such as **GAE** and **VGAE**[38], **ARGE** and **ARVGE**[30] were outperformed by either or both of **AGC** and **SSGC**. In addition, **SSGC** outperformed **SGC** [47]. Deep Embedded Clustering (**DEC**) [50], Improved Deep Embedded Clustering (**IDEC**)[12], **MGAE**[44], and Deep Attentional Embedded Graph Clustering (**DAEGC**)[43] were outperformed by **SDCN** as baselines, **GALA** [31] was outperformed by **AGE** [9] and finally **MVGRL** [14] was outperformed by **GCA** [58].

All baseline codes used are summarized in Table 9.

Table 9: URLs of GnnBP precomputation and baseline codes

Framework	URL
GnnBP	https://github.com/chennnM/GBP
DeepWalk	https://github.com/phanein/deepwalk
SDCN	https://github.com/bdy9527/SDCN
ProGCL	https://github.com/junxia97/ProGCL
AGC	https://github.com/karenlatong/AGC-master
SSGC	https://github.com/allenhaozhu/SSGC
AGE	https://github.com/thunlp/AGE
DGI	https://github.com/PetarV-/DGI
GCA	https://github.com/CRIPAC-DIG/GCA

References

1. Arora, S., Khandeparkar, H., Khodak, M., Plevrakis, O., Saunshi, N.: A theoretical analysis of contrastive unsupervised representation learning. *International Conference on Machine Learning* (2019)
2. Bo, D., Wang, X., Shi, C., Zhu, M., Lu, E., Cui, P.: Structural deep clustering network. *WWW* (2020)
3. Bromley, J., Guyon, I., LeCun, Y., Säckinger, E., Shah, R.: Signature verification using a” siamese” time delay neural network. *NeurIPS* (1993)
4. Chen, B., Li, P., Yan, Z., Wang, B., Zhang, L.: Deep metric learning with graph consistency. In: *AAAI*. vol. 35, pp. 982–990 (2021)
5. Chen, M., Wei, Z., Ding, B., Li, Y., Yuan, Y., Du, X., Wen, J.: Scalable graph neural networks via bidirectional propagation. In: *NeurIPS* (2020)
6. Chen, T., Kornblith, S., Norouzi, M., Hinton, G.: A simple framework for contrastive learning of visual representations. In: *ICML* (2020)
7. Chopra, S., Hadsell, R., LeCun, Y.: Learning a similarity metric discriminatively, with application to face verification. In: *CVPR*. IEEE (2005)
8. Chuang, C.Y., Robinson, J., Lin, Y.C., Torralba, A., Jegelka, S.: Debiased contrastive learning. *NeurIPS* (2020)
9. Cui, G., Zhou, J., Yang, C., Liu, Z.: Adaptive graph encoder for attributed graph embedding. In: *KDD* (2020)
10. Cui, Y., et al: Fine-grained categorization and dataset bootstrapping using deep metric learning with humans in the loop. In: *CVPR* (2016)
11. Goodfellow, I., Bengio, Y., Courville, A.: *Deep Learning*. MIT Press (2016), <http://www.deeplearningbook.org>
12. Guo, X., Gao, L., Liu, X., Yin, J.: Improved deep embedded clustering with local structure preservation. In: *IJCAI* (2017)
13. Hartigan, J.A., Wong, M.A.: A k-means clustering algorithm. *Journal of the Royal Statistical Society. Series C (Applied Statistics)* **28**(1), 100–108 (1979)
14. Hassani, K., Khasahmadi, A.H.: Contrastive multi-view representation learning on graphs. In: *International Conference on Machine Learning*. pp. 4116–4126. PMLR (2020)
15. Hjelm, D., Fedorov, A., Lavoie-Marchildon, S., Grewal, K., Bachman, P., Trischler, A., Bengio, Y.: Learning deep representations by mutual information estimation and maximization. In: *ICLR* (2019)
16. Khorasani, F., Gupta, R., Bhuyan, L.N.: Scalable simd-efficient graph processing on gpus. In: *PACT* (2015)
17. Khosla, P., Teterwak, P., Wang, C., Sarna, A., Tian, Y., Isola, P., Maschinot, A., Liu, C., Krishnan, D.: Supervised contrastive learning. In: *NeurIPS* (2020)
18. Klicpera, J., Bojchevski, A., Günnemann, S.: Predict then propagate: Graph neural networks meet personalized pagerank. In: *ICLR* (2019)
19. Lazer, D., Pentland, A., Adamic, L., Aral, S., Barabasi, A., Brewer, D., Christakis, N., Contractor, N., Fowler, J., Gutmann, M.: Life in the network: The coming age of computational social science **323** (2009)
20. Li, P., Chien, E., Milenkovic, O.: Optimizing generalized pagerank methods for seed-expansion community detection. *NIPS* (2019)
21. Li, Q., Han, Z., Wu, X.: Deeper insights into graph convolutional networks for semi-supervised learning. In: *AAAI* (2018)
22. Liu, Y., Tu, W., Zhou, S., Liu, X., Song, L., Yang, X., Zhu, E.: Deep graph clustering via dual correlation reduction. In: *Proc. of AAAI* (2022)

23. Loshchilov, I., Hutter, F.: Decoupled weight decay regularization. In: ICLR (2019)
24. McAuley, J., Targett, C., Shi, Q., van den Hengel, A.: Image-based recommendations on styles and substitutes. In: SIGIR (2015)
25. Meyer, B.J., Harwood, B., Drummond, T.: Deep metric learning and image classification with nearest neighbour gaussian kernels. In: ICIP (2018)
26. Newman, M.E.J.: Modularity and community structure in networks. *Proceedings of the National Academy of Sciences* **103**(23) (May 2006)
27. Norouzi, M., Fleet, D.J., Salakhutdinov, R.R.: Hamming distance metric learning. *Advances in neural information processing systems* **25** (2012)
28. Oh Song, H., Xiang, Y., Jegelka, S., Savarese, S.: Deep metric learning via lifted structured feature embedding. In: CVPR. pp. 4004–4012 (2016)
29. Oord, A.V.D., Li, Y., Vinyals, O.: Representation learning with contrastive predictive coding (2019)
30. Pan, S., Hu, R., Long, G., Jiang, J., Yao, L., Zhang, C.: Adversarially regularized graph autoencoder for graph embedding. In: IJCAI (2018)
31. Park, J., Lee, M., Chang, H., Lee, K., Choi, J.: Symmetric graph convolutional autoencoder for unsupervised graph representation learning. In: ICCV (2019)
32. Perozzi, B., Al-Rfou, R., Skiena, S.: Deepwalk: Online learning of social representations. In: KDD (2014)
33. Schroff, F., Kalenichenko, D., Philbin, J.: Facenet: A unified embedding for face recognition and clustering. CVPR (2015)
34. Sen, P., Namata, G., Bilgic, M., Getoor, L., Gallagher, B., Eliassi-Rad, T.: Collective classification in network data. Tech. rep. (2008)
35. Shchur, O., Mumme, M., Bojchevski, A., Günnemann, S.: Pitfalls of graph neural network evaluation (2019)
36. Sohn, K.: Improved deep metric learning with multi-class n-pair loss objective. In: *Advances in Neural Information Processing Systems* (2016)
37. Taubin, G.: A signal processing approach to fair surface design. In: SIGGRAPH (1995)
38. Thomas, K.N., Max, W.: Variational graph auto-encoders. NIPS Workshop on Bayesian Deep Learning (2016)
39. Thomas, K.N., Welling, M.: Semi-supervised classification with graph convolutional networks. In: ICLR (2017)
40. Tian, Y., Krishnan, D., Isola, P.: Contrastive multiview coding. In: *Computer Vision – ECCV 2020* (2020)
41. Van Der Maaten, L.: Accelerating t-sne using tree-based algorithms. *J. Mach. Learn. Res.* **15**(1), 3221–3245 (Jan 2014)
42. Veličković, P., Fedus, W., Hamilton, W.L., Liò, P., Bengio, Y., Hjelm, R.: Deep Graph Infomax. In: ICLR (2019)
43. Wang, C., Pan, S., Hu, R., Long, G., Jiang, J., Zhang, C.: Attributed graph clustering: A deep attentional embedding approach. In: IJCAI (2019)
44. Wang, C., Pan, S., Long, G., Zhu, X., Jiang, J.: Mgae: marginalized graph autoencoder for graph clustering. In: CIKM (2017)
45. Wang, F., Liu, H.: Understanding the behaviour of contrastive loss. In: CVPR (2021)
46. Wang, T., Isola, P.: Understanding contrastive representation learning through alignment and uniformity on the hypersphere. In: ICML (2020)
47. Wu, F., Souza, A., Zhang, T., Fifty, C., Yu, T., Weinberger, K.: Simplifying graph convolutional networks. In: Chaudhuri, K., Salakhutdinov, R. (eds.) *Proceedings of the 36th International Conference on Machine Learning*. *Proceedings of Machine Learning Research*, vol. 97. PMLR, 2018

- Learning Research, vol. 97, pp. 6861–6871. PMLR (09–15 Jun 2019), <http://proceedings.mlr.press/v97/wu19e.html>
48. Wu, Z., Xiong, Y., Yu, S., Lin, D.: Unsupervised feature learning via non-parametric instance discrimination. In: CVPR (2018)
 49. Xia, J., Wu, L., Wang, G., Chen, J., Li, S.Z.: Progcl: Rethinking hard negative mining in graph contrastive learning. In: ICML (2022)
 50. Xie, J., Girshick, R., Farhadi, A.: Unsupervised deep embedding for clustering analysis. In: ICML (2016)
 51. Yang, J., Leskovec, J.: Defining and evaluating network communities based on ground-truth. In: KDD. MDS '12 (2012)
 52. Ying, R., He, R., Chen, K., Eksombatchai, P., Hamilton, W.L., Leskovec, J.: Graph convolutional neural networks for web-scale recommender systems. In: KDD (2018)
 53. Yoshida, T., Takeuchi, I., Karasuyama, M.: Distance metric learning for graph structured data. *Machine Learning* **110**(7), 1765–1811 (2021)
 54. Zhang, X., Liu, H., Li, Q., Wu, X.: Attributed graph clustering via adaptive graph convolution. In: IJCAI (2019)
 55. Zhao, H., Yang, X., Wang, Z., Yang, E., Deng, C.: Graph debiased contrastive learning with joint representation clustering. In: IJCAI. pp. 3434–3440 (2021)
 56. Zhao, W., Rao, Y., Wang, Z., Lu, J., Zhou, J.: Towards interpretable deep metric learning with structural matching. In: Proceedings of the IEEE/CVF International Conference on Computer Vision (2021)
 57. Zhu, H., Koniusz, P.: Simple spectral graph convolution. In: ICLR (2021)
 58. Zhu, Y., Xu, Y., Yu, F., Liu, Q., Wu, S., Wang, L.: Graph contrastive learning with adaptive augmentation. In: WWW (2021)